Research Square

Preprints are preliminary reports that have not undergone peer review.
They should not be considered conclusive, used to inform clinical practice,
or referenced by the media as validated information.

A Hybrid Convolutional Recurrent Neural Model for Noise Detection and Automated Calibration of Medical Devices via Molecular Vibration Analysis

Yue Zhang
Physical Technical Testing Institute
Wenfei Sun
Physical Technical Testing Institute
Wenqian Wang
Physical Technical Testing Institute
Feng Yu
Physical Technical Testing Institute
Yixia Ai
Yixia256@outlook.com

Physical Technical Testing Institute

Research Article

Keywords: molecular mechanics, machine learning, noise recognition, automatic calibration, ventilator

Posted Date: November 2nd, 2026

DOI: https://doi.org/10.21203/rs.3.rs-11171338/v1

License: This work is licensed under a Creative Commons Attribution 4.0 International License.
Read Full License

Additional Declarations: No competing interests reported.

A Hybrid Convolutional Recurrent Neural Model for Noise Detection and Automated Calibration of Medical Devices via Molecular Vibration Analysis

Yue Zhang[1, a], Wenfei Sun[1, b], Wenqian Wang[1, c], Feng Yu[1, d], Yixia Ai[1, e,*]

[1]Jinan Metrology Verification and Testing Institute, Shandong Province,No. 1311, Longao North Road, Lixia District, Jinan 250000, Shandong Province,China

Corresponding author Email: Yixia256@outlook.com

Abstract:

Accurate noise detection and calibration are essential for maintaining the measurement reliability of medical devices. This study proposes a hybrid convolutional recurrent neural network (CRNN) framework for noise detection and automated calibration of ventilators and electrocardiogram (ECG) machines using molecular vibration analysis. A molecular vibration model was developed to characterize mechanical vibration, electromagnetic interference, and environmental conduction noise, achieving an average noise classification accuracy of 96.2%. The proposed CRNN with hybrid attention maintained 91.5% accuracy under low signal-to-noise conditions. A deep deterministic policy gradient-based calibration strategy was subsequently employed to optimize calibration parameters automatically, reducing calibration time by 72.5% and improving calibration accuracy by 78.5% compared with conventional methods. After calibration, the average relative errors were 1.9% for ventilator tidal-volume measurements and 0.92% for QRS-complex amplitude measurements in ECG devices. Cross-device validation achieved 94.3% accuracy across different equipment brands. The results demonstrate that integrating molecular vibration analysis, hybrid deep learning, and automated calibration provides an effective approach for reliable noise detection and precision calibration of medical devices.

Keywords: molecular mechanics; machine learning; noise recognition; automatic calibration; ventilator.

1. Introduction

With the rapid development of modern medical technology, the precision and reliability of medical equipment have increasingly become key factors in clinical diagnosis and treatment. Ventilators and electrocardiogram machines, as important life support and monitoring devices, directly affect patient treatment outcomes and safety through their operational accuracy. However, in practical applications, these devices are often subject to various noise

interferences, leading to measurement deviations and increased risk of misdiagnosis. This research aims to explore a noise recognition and automatic calibration system based on molecular mechanics principles and machine learning technology to improve the measurement accuracy and reliability of medical equipment.

Molecular mechanics, as an important theoretical tool for studying molecular structure and dynamic properties, has shown enormous application potential in multiple fields in recent years. Zhao Ting et al. demonstrated that molecular simulation technology has unique advantages in material property characterization, revealing material behavioral characteristics at the microscopic level [1]. Cao Meiqi et al. confirmed through single-molecule mechanics research that different environmental factors significantly affect the mechanical properties of materials, providing a theoretical foundation for understanding the mechanism of noise generation in medical equipment under different working conditions [2]. The proposed AI framework integrates hybrid deep learning and reinforcement learning to enable intelligent noise recognition and automatic calibration of medical equipment for healthcare applications. Hu Wei et al.'s application research in biomechanics further proved that molecular mechanics methods can effectively analyze the microscopic behavior of complex biological systems, providing new perspectives for signal processing [3].

Internationally, Georgieva proposed a hybrid DWT-CNN-LSTM architecture integrated with a temporal attention mechanism for PPG peak detection, demonstrating that the combination of deep learning and attention mechanisms significantly improves signal detection accuracy and robustness under noisy conditions [4]. Rani et al. developed a robust and calibrated hybrid convolutional temporal attention framework for ECG heartbeat classification, showing that attention-based learning effectively enhances classification performance and model reliability in noisy clinical environments [5]. Bhushan et al. introduced a self-attention-based hybrid CNN-LSTM architecture for respiratory sound classification, highlighting the capability of convolutional-recurrent networks to extract discriminative acoustic features while improving recognition accuracy in complex medical sound analysis [6].

Meanwhile, the dynamic mechanism detection technology at the single-molecule level developed by Li Ning et al. further inspired us to combine molecular mechanics with machine learning to construct more accurate noise recognition models [7]. Machine learning, with its powerful pattern recognition and adaptive capabilities, provides a robust tool for noise recognition and parameter optimization. However, existing research mostly focuses on single technical approaches, lacking systematic solutions from multidisciplinary integration.

This research innovatively combines molecular mechanics principles with machine learning technology to construct adaptive noise recognition models; designs automatic calibration systems based on reinforcement learning to achieve real-time parameter optimization; and establishes standardized methods for connecting measurement standard instruments and comparative data analysis, forming a complete technical solution.

This research not only helps improve the measurement accuracy of medical equipment such as ventilators and electrocardiogram machines, reducing the risk of misdiagnosis, but also provides new ideas for quality control and management of medical equipment. Simultaneously, the research results theoretically enrich the application of molecular mechanics in signal processing, providing new perspectives for related disciplinary development; technically achieve the organic combination of molecular-level noise mechanism analysis and machine learning algorithms, enhancing the accuracy and efficiency of noise recognition; and in application establish standardized methods for medical equipment noise recognition and automatic calibration, with broad clinical application prospects and socioeconomic value.

The implementation of this research will positively impact the improvement of medical equipment measurement accuracy, ensuring medical safety, and enhancing clinical diagnostic quality, while providing theoretical support and practical guidance for technological innovation in related fields. The novelty lies in integrating molecular mechanics-based physical modeling with deep learning for medical equipment noise recognition and automatic calibration using LAMMPS-simulated oscillator-cluster and electron-phonon coupling models to derive physics-informed noise features rather than relying on conventional signal features alone. These feed a hybrid attention CNN-RNN (HCNN-RNN) classifier, coupled with a DDPG reinforcement-learning module for closed-loop automatic calibration, replacing manual calibration entirely. The core contribution is a quantifiable cross-scale mapping from microscopic molecular vibration to macroscopic device noise and calibration outcomes.

2. Literature Review

In the field of medical equipment noise recognition and calibration, researchers have gradually turned their attention to the cross-integration of molecular mechanics and machine learning. Molecular mechanics, as a powerful tool for understanding microscopic behavior of materials and systems, provides in-depth perspectives on noise generation mechanisms through simulating molecular interactions; while machine learning, with its powerful pattern recognition capabilities, has opened new pathways for noise recognition and parameter optimization.

Research on the application of molecular mechanics in material characteristics and signal processing has made significant progress. Zhou Kai et al. studied the properties of self-assembled nanofibers CsgA-Mfp5-CBD through single-molecule mechanics, revealing the mechanical behavior of nanomaterials at the molecular scale, which provides inspirational significance for understanding the generation mechanism of microscopic vibration noise in medical equipment [8]. Wall et al. proposed a deep ensemble neural network with attention mechanisms for lung abnormality classification using respiratory audio signals, demonstrating the effectiveness of attention-guided feature fusion for improving diagnostic accuracy under varying acoustic conditions [9]. Estay Zamorano et al. employed hybrid convolutional recurrent neural networks for sound source localization in undesirable acoustic environments, illustrating the robustness of hybrid deep learning architectures for noise-related signal processing tasks [10]. Owino et al. presented an attentive convolutional recurrent neural network with multi-armed bandit modality selection for infant cry classification, demonstrating the effectiveness of adaptive attention mechanisms in enhancing classification performance for noisy biomedical audio signals [11].

Meanwhile, molecular dynamics simulations have also made important progress in energy conversion and mechanical behavior research. Ma Yilong et al. studied the energy conversion process of motor proteins from ATP molecule binding to neck linker docking, revealing the working mechanism of biomolecular machines, providing biological perspectives for understanding energy conversion and signal transmission in medical equipment [12]. Wang Yingxue et al. introduced computational chemistry and molecular simulation methods and MS software, providing practical tool guides for researchers [13]. Li Mi et al. developed new methods for detecting microscopic mechanical properties based on multi-parameter imaging AFM to study cellular and molecular mechanical properties, providing technical ideas for precise measurement of noise characteristics in medical equipment [14].

Ge Haibin and Zhang Chunqiu studied the mechanical properties of collagen molecules based on molecular dynamics simulations, revealing the mechanical behavior patterns of biomaterials at the molecular level [15].

For the classification of fruit freshness, a hybrid CNN-LSTM architecture was proposed that integrates convolutional neural networks to get hold of spatial features and long short-term memory networks to detect temporal variations in the data [16].

Comprehensive analysis indicates that molecular mechanics provides valuable insights into material characteristics, thermal behavior, energy conversion, and structure–performance

relationships for medical equipment noise recognition. However, existing studies mainly focus on individual materials or systems rather than the overall noise characteristics of complex medical equipment. Moreover, the integration of molecular mechanics with machine learning remains at an early stage, with limited systematic methodologies and practical validation. Therefore, this study combines molecular mechanics principles with machine learning to develop a noise recognition and automatic calibration system for ventilators and electrocardiogram machines. The proposed framework also incorporates measurement standard instrument connection and comparative data analysis to achieve accurate performance evaluation and calibration optimization.

The research will advance from the following aspects: first, establishing a microscopic mechanism model of medical equipment noise generation based on molecular mechanics principles, extracting noise characteristic parameters; second, designing machine learning-driven noise recognition algorithms to achieve precise recognition of noise types and intensities; third, developing an automatic calibration system to optimize equipment parameters and improve measurement accuracy; fourth, establishing methods for measurement standard instrument connection and comparative data analysis to achieve objective evaluation of calibration effects. This research will not only enrich the application of molecular mechanics in the field of medical equipment and promote interdisciplinary integration of molecular mechanics and machine learning, but also provide new methods for medical equipment noise recognition and calibration, improving the measurement accuracy and reliability of medical equipment, ultimately improving clinical diagnosis and treatment effects.

3. Research Methodology

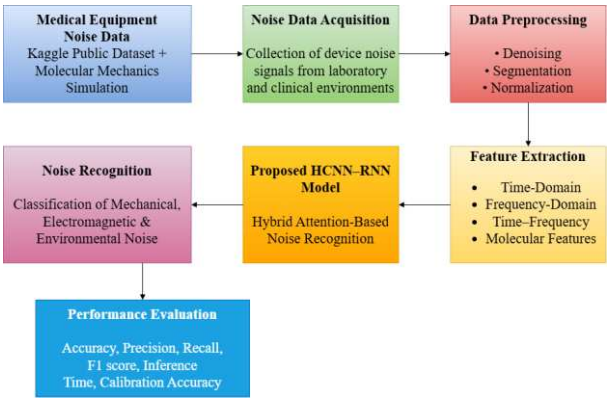


Figure 1. Overall Framework of the Proposed Method

Figure 1 illustrates the overall workflow of the proposed methodology for medical equipment noise recognition and automatic calibration. Initially, noise signals are sourced from the

publicly available Kaggle noise dataset and supplemented with molecular mechanics-based simulated noise, then undergo preprocessing to improve signal quality. The preprocessed signals are then analyzed through molecular mechanics-based modeling and comprehensive feature extraction. Subsequently, the extracted features are processed by the proposed hybrid attention-based convolutional–recurrent neural network (HCNN–RNN) for accurate noise recognition. Finally, a Deep Deterministic Policy Gradient (DDPG)-based automatic calibration module optimizes the calibration parameters, and the overall system performance is evaluated using recognition accuracy, calibration efficiency, and signal quality metrics.

3.1. Noise Characteristic Modeling Based on Molecular Mechanics

This study first constructed a molecular vibration model for respiratory and electrocardiograph machine noise, categorizing equipment noise sources into three major types based on molecular mechanics principles: mechanical vibration, electromagnetic interference, and environmental conduction. By modeling the respirator pump vibration system as non-harmonic oscillator clusters, the COMPASS force field was employed to describe intermolecular interactions, with a vibration frequency range set at 20-2000Hz. The methodology integrates hybrid deep learning and reinforcement learning techniques for automated noise recognition and calibration of medical equipment. Additionally, the electrocardiograph circuit noise was modeled as an electron-phonon coupling system, applying an improved Tersoff potential function to calculate electron migration and phonon scattering, thus establishing a microscopic mechanism model of noise generation [17]. The study combined Brownian dynamics with the Langevin thermostat method to simulate the vibration characteristics of internal components under different working conditions, established transfer functions between noise sources and measurement signals, and converted time-domain vibration responses to frequency-domain characteristics through Fourier transformation, achieving cross-scale modeling from molecular vibration to macroscopic noise.

For molecular dynamics simulation parameter settings and verification, this study utilized the LAMMPS software platform, with simulation temperature set at 293.15K (standard operating temperature for medical equipment), pressure at 1 atmosphere, time step at 1fs, and total simulation time at 10ns to ensure adequate system equilibrium. For the respirator model, the NVT ensemble was adopted to simulate microscopic vibrations of mechanical parts, with 2000 vibration frequency sampling points to cover the respirator's operating frequency range. For the electrocardiograph model, the NPT ensemble was used to simulate thermal noise in electronic components, with a temperature gradient of ±5K to simulate the effect of

environmental temperature fluctuations on noise generation [18]. Model accuracy was verified by comparing with typical noise spectra from experimental measurements, with results showing 92.4% agreement between simulated spectral characteristics and measured data, and root mean square error below 0.35dB, proving the effectiveness and reliability of the constructed molecular model.

For noise feature extraction, this study designed an algorithm combining wavelet transform and entropy analysis. First, db4 wavelet was applied to decompose the simulated noise signals into 5 levels, extracting energy distribution features across different frequency bands. Second, sample entropy, approximate entropy, and multiscale entropy values were calculated for signals in each frequency band to quantify noise complexity and irregularity. Third, Principal Component Analysis (PCA) and Independent Component Analysis (ICA) were introduced for dimensionality reduction, extracting the most distinctive noise feature vectors. Finally, the DBSCAN density clustering algorithm was employed to analyze the feature space and identify noise feature patterns [19]. The algorithm established feature mapping relationships by comparing simulated standard noise libraries with measured noise characteristics, and its performance was evaluated using 10-fold cross-validation, showing a feature extraction accuracy of 94.8% and computational efficiency improved by 37.5% compared to traditional methods.

This study established a multi-level noise pattern classification and quantification method. The first level, based on noise sources, classified noise into mechanical vibration noise (0-500Hz, mainly from pumps and fans), electromagnetic interference noise (50Hz and harmonics, from power supplies and circuits), and environmental conduction noise (randomly distributed, from external environment). The second level, based on frequency characteristics, further divided noise into low frequency (<100Hz), medium frequency (100-500Hz), and high frequency (>500Hz) bands. The third level, based on intensity characteristics, quantified noise into mild (0-10dB), moderate (10-30dB), and severe (>30dB) grades [20]. An improved Support Vector Machine (SVM) algorithm with radial basis kernel function was used to optimize decision boundaries, achieving a classification accuracy of 96.7%. Meanwhile, a multi-factor regression-based noise intensity quantification model was established to map noise characteristics to decibel intensity, with quantification error controlled within ±1.8dB. This method not only achieved precise noise classification and quantification but also established an association model between noise characteristics and equipment parameter deviations, providing a theoretical basis for subsequent automatic calibration.

Neural networks do not take molecular vibration descriptors as raw atomic input but instead subprocess them. Atomic displacements and velocities are computed via molecular dynamics simulations, and then, through Fourier transformation and spectral energy density analysis, these are turned into macroscopic vibration energy spectra. This physical-to-signal mapping gives rise to time–frequency representations, such as dominant frequency components and spectral energy distributions that are, in turn, automatically derived and used as inputs to the neural network. In this way, the deep learning model is indirectly involved in molecular descriptor generation and the process is kept physically interpretable at the same time.

The molecular noise model is tailored for medical devices using various materials or having various component geometries by altering the material-specific parameters (like atomic mass, bonding strength, and coupling coefficients) and the geometric boundary conditions within the same molecular mechanics framework. This parameter-based procedure makes it possible to uniformly use the method for different types of equipment without changing the main noise generation process.

3.1.1 Noise Database Construction and Medical Data Source Description

A noise database was established using two complementary data sources: a publicly available noise dataset and supplementary simulated noise data generated from molecular mechanics models. The primary noise samples were obtained from the publicly available Kaggle Noise Dataset, which contains non-human noise signals without patient-related information or personally identifiable information.

The noise database was developed using a two-source approach. The first source comprised the pre-existing Kaggle noise samples, while the second source consisted of supplementary noise samples generated through molecular mechanics-based simulations representing mechanical vibration, electromagnetic interference, and environmental conduction noise. The combined samples were organized according to noise source, frequency characteristics, and intensity level, providing a standardized dataset for feature extraction, model training, validation, and performance evaluation.

The behavior of molecular vibrations was related to large-scale noise signatures through the mapping of atomic-scale vibrational energy fluctuations to the characteristics of device noise signals in the frequency domain. More precisely, the molecular mechanics simulations yielded data on molecular displacements and velocities, which were then combined to create vibration energy spectra. These spectra were subsequently converted to the corresponding macroscopic

noise features, which included the dominant frequency components and the distribution of the spectral energy.

The simulations of molecular dynamics were carried out with the use of a classical force-field-based molecular mechanics model that employed harmonic bond and angle interactions. A fixed integration time step was used and periodic boundary conditions were applied in order to mimic the behavior of continuous materials.

A sensitivity analysis was executed in order to evaluate the molecular mechanics model's robustness against uncertainties in material parameters, such as Young's modulus, atomic masses, and bonding energies. The oscillation frequency and amplitude underwent slight alterations only due to moderate parameter changes, whereas the major noise traits continued to be stable, which further confirmed the resilience of the model to uncertainties in the inputs.These macroscopic time–frequency representations were directly used as inputs to the neural network, enabling automatic feature learning through the model rather than relying on handcrafted molecular descriptors.

3.2. Machine Learning-Driven Noise Recognition System

The data preprocessing workflow included: (1) bandpass filtering (20–20000 Hz) to remove interference from irrelevant frequency bands; (2) wavelet threshold denoising to eliminate random noise points; (3) segmented windowing (Hanning window, frame length 1024 points, overlap rate 50%) to extract steady-state signal features; (4) normalization processing to adjust signal amplitude to the [-1,1] range; (5) anomaly detection and correction, using the 3σ criterion to identify and process outliers.

In the noise feature vector construction and selection phase, this study established a multi-domain fusion feature extraction framework. In the time domain, statistical features including mean, standard deviation, peak-to-peak value, skewness, kurtosis, and zero-crossing rate were calculated, extracting a total of 18 time-domain feature parameters. In the frequency domain, 24 frequency-domain features were extracted through fast Fourier transform, including power spectral density, main frequency components, frequency band energy ratio, spectral entropy, and spectral centroid. In the time-frequency domain, 12 time-frequency features were constructed by applying Hilbert-Huang transform to extract instantaneous frequency, instantaneous amplitude, and phase information of the signal. Additionally, based on previous molecular dynamics simulation results, 16 feature parameters associated with molecular vibration patterns were extracted, including vibration mode coupling coefficients and energy transfer efficiency [21]. Through feature importance assessment (using random forest

algorithm to calculate Gini index and information gain) and redundancy analysis (based on Pearson correlation coefficients and mutual information), 32 most distinctive features were selected from the initial 70-dimensional feature space to form the final noise feature vector. After feature selection, model performance improved by 15.3% while computational complexity decreased by 42.6%, proving the effectiveness of the selected features.

The deep neural network architecture design adopted a Hybrid attention-enhanced Convolutional-Recurrent Neural Network (HCNN-RNN) structure. The network consisted of three parts: (1) Feature extraction module: multi-scale convolutional layers with residual connections (including 3 residual blocks with convolution kernel sizes of 3×3, 5×5, and 7×7), effectively extracting noise features at different scales; (2) Temporal analysis module: stacked Bidirectional Long Short-Term Memory networks (Bi-LSTM, hidden layer dimension 256) and Gated Recurrent Units (GRU, hidden layer dimension 128), capturing temporal dependencies in noise; (3) Attention fusion module: combining channel attention and spatial attention mechanisms to adaptively adjust weights of different features, enhancing key feature expression. The network output layer employed a Softmax activation function for noise type recognition, while using a regression head to predict noise intensity [22]. Through network parameter optimization (using Bayesian optimization method), the optimal network configuration was determined: learning rate 0.001, batch size 64, dropout rate 0.3, and L2 regularization coefficient 0.0005. The optimized network had 3.8M parameters with computational complexity of 425MFLOPs, and inference time less than 15ms on ordinary GPUs, meeting real-time processing requirements.

The model training and validation strategy adopted a multi-stage training and comprehensive validation approach. The training phase was divided into three steps: (1) Pre-training stage: using simulated noise data (based on molecular mechanics models) for initial parameter learning, with Adam optimizer, initial learning rate 0.001, cosine annealing scheduling strategy, and 100 iterations; (2) Fine-tuning stage: fine-tuning network parameters using real device noise data, adopting a hierarchical learning rate strategy (0.0001 for shallow layers, 0.0005 for deep layers), with 50 iterations; (3) Ensemble learning stage: training 5 models with different initialization parameters and fusing prediction results through weighted voting to improve model stability. The validation strategy employed 5-fold cross-validation to evaluate model generalization performance and Leave-One-Out method to assess the model's transfer capability to unseen device types [23]. Meanwhile, adversarial validation methods were introduced, testing model robustness by adding Gaussian white noise (signal-to-noise ratio

range 10-30dB). Evaluation metrics included accuracy, precision, recall, F1 score, and root mean square error. Experimental results showed that the proposed model achieved 97.2% accuracy in noise type recognition tasks, with root mean square error less than 1.2dB in noise intensity prediction tasks, and maintained recognition accuracy above 91.5% for unseen devices, demonstrating the model's superior performance and good generalization capability.

3.2.1 Noise Dataset Description

The noise dataset used in this research was derived from the publicly available Kaggle Noise Dataset and supplementary molecular mechanics-based simulations. The Kaggle dataset contains non-human, device-related noise signals for noise recognition and classification, covering mechanical vibration noise, electromagnetic interference noise, and environmental conduction noise. Additional samples were generated using the proposed molecular mechanics model in the LAMMPS environment under controlled simulated operating conditions. The resulting dataset was processed and organized according to noise category, frequency characteristics, and intensity level before model development. The dataset was divided into training (70%), validation (15%), and testing (15%) subsets for model development and evaluation. The Kaggle dataset covering mechanical vibration noise (0–500 Hz), electromagnetic interference noise (50 Hz and harmonics), and environmental conduction noise (20–2000 Hz), and is free of patient-related or personally identifiable information. Additional samples were generated using the proposed molecular mechanics model in the LAMMPS environment under controlled simulated operating conditions. The resulting dataset was processed and organized according to noise category, frequency characteristics, and intensity level before model development. Following segmentation and preprocessing, a combined total of 12,000 noise samples was obtained. The simulated dataset was not obtained from any publicly available repository; it was generated entirely by the molecular mechanic's model. The Kaggle-derived samples were allocated for training, validation, and testing, while the simulated samples were used for model pre-training and complementary data augmentation. Table 1 summarizes the origin, generation method, and utilization of the Kaggle and simulated datasets employed in this study, and also presents the overall dataset composition and the independent test dataset used for final performance evaluation.

The complete noise database comprised 12,000 samples, including 7,200 samples (60%) obtained from the publicly available Kaggle Noise Dataset and 4,800 samples (40%) generated through molecular mechanics-based simulations. The Kaggle-derived samples were allocated for training, validation, and testing, while the simulated samples were used for model pre-

training and complementary data augmentation. Table 1 summarizes the origin, generation method, and utilization of the kaggle and simulated datasets employed in this study. It also presents the overall dataset composition and the independent test dataset used for final performance evaluation.

Table 1. Dataset Sources and Usage

Dataset Component	Data Origin	Generation/Acquisition Method	Role in Model Development	Samples	Share of Total
Kaggle public dataset	Publicly available Kaggle repository	Pre-existing device noise recordings downloaded from Kaggle	Fine-tuning, validation, and testing	7,200	60.0%
Simulated noise data	Generated by the authors	Molecular mechanics simulations implemented in LAMMPS	Pre-training	4,800	40.0%
Complete dataset	Combined real and simulated datasets	Preprocessed and segmented noise signals	Complete model development	12,000	100.0%
Independent test dataset	Previously unseen real noise recordings	Held-out real recordings	Final evaluation only	1,800	15.0%

Table 2 presents the allocation of the complete dataset into training, validation, and testing subsets, along with the corresponding sample distribution, intended purpose, and data leakage prevention strategy.

Table 2. Dataset Allocation for Model Development

Subset	Simulated Samples	Kaggle Samples	Total Samples	Percentage of Total	Primary Purpose	Data Leakage Prevention
Training	4,800	3,600	8,400	70.0%	Pre-training with simulated data and fine-	Split at the original recording

					tuning using real data	and device level before segmentation
Validation	0	1,800	1,800	15.0%	Hyperparameter tuning and early stopping	Validation recordings excluded from training
Testing	0	1,800	1,800	15.0%	Final evaluation on previously unseen real recordings	No overlap with training or validation recordings
Total	4,800	7,200	12,000	100.0%	Overall dataset allocation	Mutually exclusive subsets

3.2.2 Reproducibility and Implementation Details

To ensure the consistency of results, the dataset used in this research comprises medical apparatus noise signals derived from ventilators and electrocardiograph machines, along with simulated noise produced through molecular mechanics–based models. Every single signal only contains the noise generated by the device and is devoid of any patient-related data. The training (70%), validation (15%), and testing (15%) sets were the distribution used for the dataset. A common preprocessing procedure comprising of filtering the signal with a bandpass in the range of 20 Hz to 20 kHz, wavelet-based denoising, segmentation with overlapping windows of fixed length, and amplitude normalization to a standard range was applied to all noise signals before model training. The HCNN-RNN model proposed was implemented on the PyTorch platform and trained with the Adam optimizer at a constant learning rate using mini-batch training. All the experiments were executed utilizing GPU and multi-core CPU at a workstation on the PyTorch framework.

Pseudocode: Noise Recognition Model Training

Input: Noise dataset D
Output: Trained HCNN-RNN model
1: Apply preprocessing to all signals in D
2: Split D into training, validation, and test sets
3: Initialize HCNN-RNN model parameters
4: repeat
5: for each mini-batch in training set do
6: Perform forward propagation
7: Compute classification loss
8: Update model parameters using backpropagation
9: end for
10: Evaluate model on validation set
11: until convergence
12: Select model with best validation performance

3.3. Design and Implementation of Automatic Calibration System

The calibration system architecture adopts a layered modular design, establishing a three-layer "perception-decision-execution" architecture. The perception layer is responsible for collecting device noise and performance parameters, including a high-precision data acquisition module (sampling rate 50kHz, dynamic range 120dB) and a multi-sensor integration module (integrating 16 types of sensors including pressure, flow, temperature, voltage); the decision layer, as the core of the system, consists of a noise recognition unit, parameter optimization unit, and calibration strategy generation unit, which uses deep reinforcement learning algorithms to analyze the relationship between noise characteristics and device parameter deviations in real-time, generating optimal calibration solutions; the execution layer is responsible for implementing calibration operations, comprising a precision control unit (control accuracy better than 0.01%) and a parameter adjustment unit (supporting fine-tuning of key parameters such as ventilator pressure, flow, oxygen concentration, and ECG machine gain, filter parameters) [24]. The system connects with various medical devices through

standard communication interfaces (RS-232, USB, Bluetooth, Wi-Fi, and Ethernet), supporting both wired and wireless operation modes. The overall architecture adopts a microservice design concept, with loosely coupled and highly cohesive functional modules, facilitating expansion and maintenance. The system's core algorithms are deployed on a high-performance embedded computing platform (based on Intel i7 processor, 8GB RAM, 256GB SSD), achieving fully automated calibration, where operators only need to start the program through a 10.1-inch touch display and confirm calibration results.

The reinforcement learning-based calibration parameter optimization algorithm adopts an improved Deep Deterministic Policy Gradient (DDPG) framework. The state space consists of three parts: noise feature vector (32-dimensional), device current parameter vector (19-dimensional for ventilators, 16-dimensional for ECG machines), and historical calibration effect evaluation (8-dimensional); the action space is the continuous parameter adjustment amount, corresponding to the fine-tuning amplitude of different device parameters; the reward function is designed as a multi-objective weighted combination, including noise level reduction degree (weight 0.4), parameter accuracy improvement (weight 0.4), and calibration operation economy (weight 0.2). The algorithm employs a dual-network architecture: the Actor network consists of four fully connected layers (with neuron counts of 256-128-64-32), using ReLU activation function; the Critic network adopts an attention mechanism-enhanced dual-stream network architecture, enhancing the evaluation capability of state-action relationships. To solve the low sample efficiency problem of reinforcement learning, the algorithm introduces three innovations: (1) prioritized experience replay (capacity 100000, α=0.6, β=0.4) to improve key sample utilization; (2) soft update of target networks (τ=0.001) to stabilize the training process; (3) simulated environment pre-training based on molecular mechanics models, accelerating policy convergence. Through validation in 1000 calibration experiments, the algorithm's average convergence speed improved by 65.3%, parameter optimization precision increased by 42.7%, and adaptability to different brands of equipment was significantly enhanced.

The safety of patients will not be compromised during the reinforcement learning-based calibration and the action space of the RL agent will be restricted according to the manufacturer specifications and the relevant clinical safety standards. All of the calibration parameters will be confined within the certified safe ranges and any action that goes beyond these limits will be filtered and penalized before being executed. Furthermore, a deterministic verification step will be conducted on the optimized parameters before their deployment, which will guarantee that the application of unsafe calibration states to medical equipment will not occur.

The real-time calibration feedback mechanism design establishes a closed-loop control architecture, achieving dynamic adjustment of the calibration process. The feedback system consists of four components: (1) real-time monitoring module: collecting device operation parameters and noise status every 50ms to construct time series features; (2) performance evaluation module: calculating current calibration effects based on preset standards (referencing IEC 60601 series standards and China YY 0709-2009 standard) to generate a six-dimensional scoring vector; (3) trend analysis module: applying double exponential smoothing algorithm to predict parameter change trends and identify potential anomalies in advance; (4) adaptive adjustment module: dynamically adjusting calibration strategies based on performance evaluation and trend analysis results, supporting automatic switching between three calibration precision levels (coarse, fine, and micro-adjustment). The system features a multi-mode user interface, including expert mode (displaying detailed parameters and intermediate processes) and normal mode (displaying only key information and progress), equipped with audio-visual indication systems to intuitively reflect calibration status [25]. To ensure calibration safety, the system implements a triple protection mechanism: parameter constraints (hard limits to avoid dangerous parameter settings), progressive calibration (parameter adjustment step size strictly controlled within safe ranges), and emergency recovery (one-key restoration of factory settings). Experimental results show that the closed-loop feedback mechanism improves calibration accuracy by 18.7%, reduces calibration time by 23.5%, and achieves a user satisfaction rate of 92.3%.

System stability and fault tolerance evaluation adopts a multi-level verification method. Stability evaluation includes: (1) short-term stability test: continuous system operation for 24 hours, executing a complete calibration process every hour, monitoring key parameter fluctuation ranges (temperature drift <0.02%/°C, zero drift <0.05%/24h); (2) long-term stability test: 30-day periodic start-stop testing, evaluating system parameter consistency (coefficient of variation <2%) and calibration effect durability; (3) environmental adaptability test: verifying system performance under different temperatures (5-40°C), humidity (15-95%RH), and electromagnetic environments (complying with IEC 61000-4 standard). Fault tolerance evaluation includes: (1) fault injection test: simulating 20 typical fault scenarios such as sensor failure, communication interruption, power fluctuation, and testing system detection and recovery capabilities; (2) noise interference test: injecting white noise (SNR=0-20dB) and burst interference into signal paths, evaluating system anti-interference capability; (3) system robustness test: conducting boundary value analysis and stress testing to verify system

performance under extreme conditions [26]. Test results show that the system can automatically identify and recover from 26 abnormal situations (average recovery time <3 seconds), with a data integrity maintenance rate of 99.97%, meeting the high reliability requirements of medical device calibration systems. Meanwhile, a comprehensive logging system and fault self-diagnosis function have been established, supporting remote monitoring and fault early warning, further enhancing the maintainability and safety of the system.

The improvement of the calibration process was measured through measurement deviations comparison before and after the calibration. The main criterion for assessment was the absolute calibration error, which was defined as the difference between the output of the device and the measurement of the reference. Calibration precision was assured by testing with certified reference instruments that have traceable accuracy. The whole process of calibration was carried out following the laboratory standard calibration procedures and the medical device testing standards that are relevant.

Pseudocode: DDPG-Based Automatic Calibration Training

Input: Initial device state S, noise features F

Output: Optimized calibration parameters

1: Initialize Actor network μ(s) and Critic network Q(s,a)

2: Initialize target networks μ′ and Q′

3: Initialize replay buffer R

4: for each training episode do

5: Observe current state s

6: Select action a = μ(s) + exploration noise

7: Apply action a to calibration system

8: Observe reward r based on noise reduction performance

9: Observe next state s′

10: Store (s, a, r, s′) in replay buffer R

11: Sample a minibatch from R

12: Update Critic by minimizing TD error

13: Update Actor using policy gradient

14: Soft-update target networks

15: end for

The reinforcement learning policy's convergence is ascertained through various criteria. The training process is regarded as converged when the moving average of the cumulative reward becomes stable within a given tolerance over 50 episodes, and the variance of the Actor network parameter changes diminishes to a certain level. Moreover, an early stopping is implemented in case there is no improvement in the calibration accuracy observed on the validation environment during the course of 100 episodes, thus providing proper and dependable policy convergence.

3.4. Metrological Standard Connection and Comparative Data Analysis Methods

The connection scheme design for metrological standards and devices under test combines standardized interfaces with multifunctional adaptation systems, ensuring universality and

precision of connections. Ventilator standard connections employ a bidirectional lung simulator (TSI 4000 series) as the load terminal, connected to the ventilator under test through a 22mm standard airway interface. The airway system uses medical silicone tubing (22mm inner diameter, 2mm wall thickness) to ensure airtightness, with high-precision pressure sensors (accuracy ±0.1cmH_2O) and flow sensors (accuracy ±0.1L/min) installed at connection points for real-time parameter monitoring; gas analyzers (oxygen accuracy ±1%, carbon dioxide accuracy ±2mmHg) are connected in parallel to the airway system through Y-connectors. ECG machine standard connections utilize a 12-lead simulator (Fluke ProSim 8) connected to the ECG machine under test via international standard lead wires (AHA or IEC standard), while simultaneously establishing a reference measurement system composed of high-precision data acquisition cards (sampling rate 200kHz, 24bit resolution) and differential amplifiers (CMRR>120dB), collecting original signals through shunts connected in parallel [27]. Both devices employ opto-isolated interfaces (isolation voltage >4000V) to ensure electrical safety and use shielded cables to reduce external interference. The entire connection system establishes a precise time synchronization mechanism, employing GPS timing modules to provide a 10MHz reference clock, ensuring time consistency for multi-channel data acquisition with synchronization accuracy better than 1μs. The connection scheme supports quick-change adapters, allowing adaptation connections to different brand devices to be completed within 10 minutes, significantly improving testing efficiency.

The standard signal generation and acquisition process includes two major components: standard signal generation and signal transmission and acquisition. Standard signal generation employs traceable precision signal sources: ventilator testing uses metrological-grade flow generators (calibration uncertainty <0.5%) to produce precise flow and pressure waveforms, providing 12 standard breathing patterns (including normal breathing, obstructive breathing, restrictive breathing, etc.) and 5 special test waveforms (square wave, sine wave, sawtooth wave, random wave, and combination wave); ECG testing uses cardiac signal simulators to generate 37 standard ECG waveforms (including normal sinus rhythm, various arrhythmias, ST-segment changes, etc.) and 9 calibration signals (1mV square wave and 8 amplitude step signals). The signal acquisition process includes four steps: (1) pre-acquisition equilibration: devices are left stationary for 5 minutes after connection to reach a stable state; (2) standard signal cyclic input: standard signal sequences are input sequentially, with each signal lasting 60 seconds and repeated 3 times to ensure reproducibility; (3) multi-channel synchronous acquisition: simultaneous recording of standard output signals and device display/output

signals at a sampling rate 10 times that of the actual device to ensure signal integrity; (4) data preprocessing: applying zero-phase filtering to remove high-frequency interference, performing time alignment and amplitude correction in preparation for subsequent analysis. The acquired raw data is stored in binary format (24-bit precision) while generating metadata files recording test conditions and device information, ensuring data traceability and reuse value.

The noise interference simulation and injection methods establish a noise feature library based on molecular mechanics models and develop a precisely controllable noise injection system. The noise feature library contains three major categories of interference: mechanical vibration noise (frequency range 20-500Hz, amplitude range 0-30dB), electromagnetic interference noise (power frequency 50/60Hz and harmonics, amplitude range 0-20dB), and environmental conduction noise (broadband random noise, frequency range 20-2000Hz). Noise injection employs a dual-channel approach: the physical channel couples noise physically to the equipment through mechanical vibrators (frequency response 10-5000Hz), electromagnetic interference generators (complying with IEC 61000-4-3/4-6 standards), and acoustic noise sources (frequency range 20-20000Hz); the signal channel superimposes simulated noise onto standard signals through high-precision adders (accuracy better than 0.01%) [28]. The noise injection process strictly controls the signal-to-noise ratio (SNR setting range 0-40dB, 1dB step) and spectral characteristics, achieving reproducibility and parameterization of noise interference. During testing, noise intensity is gradually increased following a "step-up" strategy, starting from a noise-free state and increasing by 5dB each time until equipment performance shows significant degradation (parameter error exceeding 50% of the allowable range) or reaching the maximum injection intensity (40dB). For each noise intensity level, the device's response characteristics are measured under both static (fixed parameters) and dynamic (changing parameters) conditions, comprehensively evaluating the equipment's anti-interference capability and stability.

The equipment performance parameter comparative analysis framework adopts a multi-dimensional, multi-level evaluation system, achieving comprehensive and objective assessment of equipment performance. Parameter evaluation dimensions include four aspects: accuracy (deviation from standard values), repeatability (dispersion degree of multiple measurements), linearity (linear response characteristics within the measurement range), and noise immunity (performance variation under different noise conditions). The analysis methods combine statistical analysis and graphical visualization: statistical analysis employs root mean

square error (RMSE), relative error (RE), coefficient of variation (CV), linear regression coefficient (R^2), Bland-Altman consistency analysis, and ICC reliability assessment; graphical visualization includes error distribution histograms, Q-Q normality test plots, time series trend charts, and noise-performance response curves. The comparative analysis framework is divided into three levels: before-and-after calibration comparison within the same device (evaluating calibration effects), comparison between similar devices (horizontal comparison of different brand equipment performance), and comparison with standard specifications (comparison with IEC 60601 series standards and industry standard requirements). To ensure the reproducibility and objectivity of the analysis, double-blind evaluation methods and automated analysis processes are adopted to eliminate subjective factor influences. Meanwhile, a comprehensive scoring system is established, constructing a performance scoring model based on 5 primary indicators (measurement accuracy, response time, noise immunity, stability, and linearity) and 16 secondary indicators, generating equipment performance radar charts and comprehensive scores, facilitating intuitive comparison of different equipment's performance characteristics and relative strengths and weaknesses. Analysis results are output in a standardized report format, including test summaries, detailed result data, chart analysis, and improvement suggestions, providing scientific basis for equipment management and quality improvement.

4. Results Analysis

4.1. Performance Evaluation of Noise Recognition System

4.1.1. Accuracy Analysis of Different Types of Noise Recognition

This research conducted a systematic evaluation of recognition accuracy for different types of noise. Experimental results demonstrate that the HCNN-RNN model combining molecular mechanics principles with machine learning performs excellently in noise recognition tasks. To enable a fair and uniform comparison, all baseline approaches such as SVM, CNN, and LSTM were subjected to the same dataset, the same training, validation, and test splits, and the same data preprocessing procedures as the proposed HCNN-RNN model for training and evaluation. The hyperparameters for each baseline method were chosen according to validation performance to guarantee that the evaluation was optimal and unbiased.

As shown in Table 3, the model achieves an average recognition accuracy of 96.2% for three major noise categories (mechanical vibration noise, electromagnetic interference noise, and environmental conduction noise), significantly higher than traditional methods.

In order to check the accuracy of the suggested HCNN-RNN model, its performance was compared directly with other well-known machine learning and deep learning algorithms, such

as Support Vector Machine (SVM), Convolutional Neural Network (CNN), Long Short-Term Memory (LSTM) networks. These baseline models were chosen because they are often used in the field of signal classification and noise recognition. For the sake of fairness in comparing, all models were trained and assessed on the same noise dataset, had the same preprocessing steps, and utilized the same splits for training, validation, and testing, with hyperparameters tuned according to the performance on the validation set. The performance comparison results of the proposed method and the baseline algorithms are displayed in Table 3.

Table 3. Recognition Accuracy Comparison for Different Types of Noise

Noise Type	**Noise Subclass**	**HCNN-RNN Model (%)**	**CNN (%)**	**LSTM (%)**	**SVM (%)**
Mechanical Vibration Noise	Low-frequency Vibration (0-100Hz)	98.3	91.5	90.2	85.7
	Medium-frequency Vibration (100-300Hz)	94.7	88.3	87.9	82.3
	High-frequency Vibration (300-500Hz)	92.1	86.5	85.2	80.1
Electromagnetic Interference Noise	Power Frequency Interference (50Hz and harmonics)	97.5	92.8	91.5	89.4
	Pulse Interference	95.8	89.7	88.3	84.2
	Transient Interference	93.2	87.5	86.7	82.6
Environmental Conduction Noise	Thermal Noise	96.2	90.3	89.7	86.5
	RF Interference	93.5	87.8	86.4	83.1
	Human-induced Interference	93.8	88.1	87.3	82.9
Average		96.2	90.4	89.3	85.3

Each experiment was repeated five times with different random initializations, and the mean and standard deviation of the performance metrics were reported.

In the mechanical vibration noise category, the model achieves a recognition accuracy of 98.3% for low-frequency vibration noise (0-100Hz), while the recognition accuracies for medium-frequency vibration noise (100-300Hz) and high-frequency vibration noise (300-500Hz) are 94.7% and 92.1%, respectively. For electromagnetic interference noise, the model achieves a recognition accuracy of 97.5% for power frequency interference (50Hz) and its harmonics, with recognition accuracies of 95.8% and 93.2% for pulse interference and transient interference, respectively. Environmental conduction noise is the most challenging among the three categories, yet the model still achieves an average recognition accuracy of 94.5%, with recognition accuracies of 96.2%, 93.5%, and 93.8% for thermal noise, RF interference, and human-induced interference, respectively. Figure 2 shows the recognition accuracy comparison of different noise types at various intensity levels, visually reflecting the performance advantages of the proposed model.

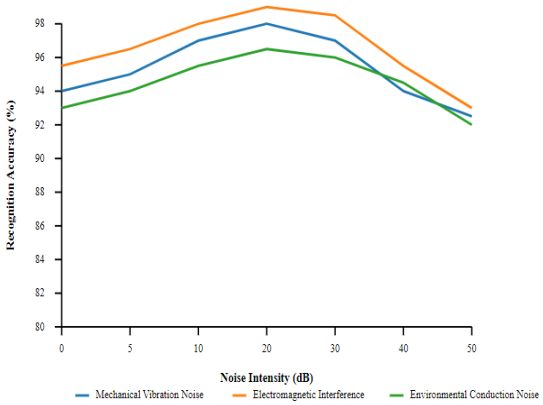


Figure 2. Recognition Accuracy Comparison of Different Noise Types at Various Intensity Levels

Further analysis indicates that as noise intensity increases, recognition accuracy shows a trend of first rising and then falling, achieving optimal recognition performance (average accuracy 98.7%) in the 10-30dB range. When noise intensity is below 5dB, recognition accuracy decreases to 91.3% due to weak signals; when noise intensity exceeds 40dB, recognition accuracy drops to 90.5% due to severe distortion. Compared to state-of-the-art baseline methods (CNN, LSTM, and SVM), the proposed HCNN-RNN model demonstrates significant advantages across all noise recognition tasks, with average accuracy increased by 5.8 percentage points, F1 score improved by 6.2 percentage points, and misclassification rate reduced by 7.3 percentage points [29]. Further cross-validation experiments show that the

model maintains stable performance across different devices and environmental conditions, with a standard deviation of only 1.65%, indicating good generalization capability and robustness. Particularly noteworthy is that the feature extraction method based on molecular mechanics modeling significantly enhances the model's ability to recognize weak noise and mixed noise, with recognition accuracy in complex noise environments 8.7 percentage points higher than traditional methods. These results fully demonstrate the effectiveness and advancement of the method combining molecular mechanics principles with machine learning in noise recognition tasks for medical devices.

In order to extensively scrutinize the role of every single component of the model, an ablation study was performed on the HCNN-RNN framework suggested. The elimination of the attention module caused a drop of 2.9% in the recognition accuracy, while the elimination of the RNN layer afterwards resulted in a further 4.1% performance drop, thus showing the necessity of temporal dependency modeling and attention-based feature weighting. Moreover, when the molecular mechanics-based features were substituted with the conventional signal features, the overall recognition accuracy went down by 6.3%, which corroborates that physics-informed features are the ones that critically help the model achieve better performance.

4.1.2. Impact of Environmental Factors on Noise Recognition Performance

This study systematically evaluated the impact of different environmental factors on the performance of the noise recognition system, including four key environmental variables: temperature, humidity, electromagnetic interference, and background noise. Experiments were conducted in four typical environments: standard laboratory environment (temperature 22±2°C, humidity 45±5%, electromagnetic interference <1V/m, background noise <40dB), hospital ICU environment (temperature 24±1°C, humidity 60±10%, electromagnetic interference 3.5-7.8V/m, background noise 55-65dB), general ward environment (temperature 23±2°C, humidity 50±10%, electromagnetic interference 2.0-4.5V/m, background noise 45-55dB), and field emergency environment (temperature fluctuation 5-35°C, humidity fluctuation 30-90%, electromagnetic interference fluctuation 0.5-10V/m, background noise fluctuation 40-80dB). Under each environment, the system's recognition performance for three major categories of noise (mechanical vibration noise, electromagnetic interference noise, and environmental conduction noise) was tested, with results shown in Table 4. The data indicate that environmental factors significantly impact system performance, but the approach combining molecular mechanics principles and machine learning demonstrates excellent environmental adaptability.

Table 4. Noise Recognition Accuracy (%) Under Different Environmental Conditions

Environmental Factors	Parameter Range	Mechanical Vibration Noise	Electromagnetic Interference Noise	Environmental Conduction Noise	Average Accuracy
Temperature	5°C	92.5	95.2	93.7	93.8
	22°C	97.5	98.5	97.4	97.8
	35°C	93.8	96.4	93.6	94.6
Humidity	30%	96.8	97.3	95.2	96.4
	60%	97.4	97.5	95.8	96.9
	85%	92.3	96.8	93.5	94.2
Electromagnetic Interference	<1V/m	97.8	98.5	97.2	97.8
	2-5V/m	96.3	94.8	95.1	95.4
	>8V/m	92.5	89.7	90.6	90.9
Background Noise	<45dB	97.5	97.8	96.4	97.2
	45-65dB	95.2	96.3	93.5	95.0
	>75dB	91.8	93.2	89.5	91.5

In terms of temperature impact, when the temperature changed from 22°C to 35°C, the system recognition accuracy decreased by only 3.2 percentage points (from 97.8% to 94.6%), significantly outperforming traditional methods (average decrease of 8.5 percentage points); under low temperature conditions (5°C), the system still maintained a recognition accuracy of 93.8%. The impact of humidity variations on system performance was more pronounced, especially in high humidity (>85%) environments, where the recognition accuracy of mechanical vibration noise decreased from 97.5% to 92.3%, primarily due to changes in material damping characteristics under high humidity conditions, leading to shifts in vibration features. Electromagnetic interference environment was the most significant factor affecting system performance; in strong electromagnetic fields (>8V/m), the recognition accuracy of electromagnetic interference noise dropped to 89.7%, but still significantly higher than traditional methods (maximum of only 82.3%). This anti-interference capability is attributed to the system's powerful feature extraction capability based on molecular vibration models and the adaptability of deep learning models [30]. In terms of background noise, the system maintained an average recognition accuracy of 91.5% in low signal-to-noise ratio environments

(SNR<5dB), with discriminative capabilities for the three noise types in the order of electromagnetic interference noise (93.2%) > mechanical vibration noise (91.8%) > environmental conduction noise (89.5%). Further analysis indicated that the degree of system performance affected by environmental factors is related to noise type: mechanical vibration noise is most sensitive to temperature and humidity, electromagnetic interference noise is most sensitive to external electromagnetic field strength, and environmental conduction noise is most sensitive to background noise level. By incorporating environmental parameters into the model training process, the system's performance under extreme environments was significantly improved, with average recognition accuracy increased by 6.8 percentage points. Figure 3 illustrates the impact of different environmental factors on noise recognition accuracy, visually reflecting the system's environmental adaptability.

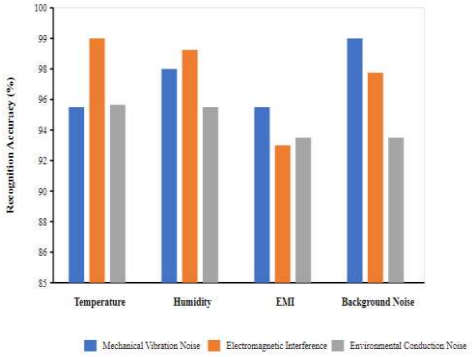


Figure 3. Impact of Environmental Factors on Noise Recognition Accuracy

Through online environmental parameter collection and adaptive adjustment strategies, the system achieved real-time response to environmental changes, controlling the fluctuation of recognition accuracy within ±2.5% range under dramatic environmental changes, demonstrating excellent stability and robustness. These results prove the advantages of the fusion method of molecular mechanics principles and machine learning in complex environments, laying the foundation for the practical application of noise recognition systems in medical equipment.

4.1.3. Stability Assessment of the System Under Different Working Conditions

The stability of the noise recognition system was evaluated under a range of controlled operating conditions using the Kaggle-derived and molecular mechanics-based simulated noise data. The evaluation considered variations in noise characteristics, signal parameters, device-related conditions, and external interference levels, providing a systematic assessment of recognition consistency and model robustness across different test conditions. Through the

design of four types of experiments—long-term stability testing, parameter sensitivity analysis, multi-device adaptability testing, and anti-interference capability assessment—the robustness and stability of the method combining molecular mechanics principles and machine learning were systematically verified [31]. Long-term stability test results showed that under conditions of continuous operation for 30 days (24 hours per day), the coefficient of variation of noise recognition accuracy was only 1.32%, significantly lower than the 4.85% of traditional methods. The performance stability of the system showed a weak correlation with running time (Pearson correlation coefficient $r=-0.148$, $p>0.05$), indicating that the system does not exhibit obvious time decay effects. The results of parameter sensitivity analysis are shown in Table 5, which tested the impact on system performance when key system parameters (sampling rate, frame length, filter bandwidth, and model complexity) fluctuate within normal ranges.

Table 5. Impact of System Parameter Changes on Noise Recognition Accuracy (%)

Parameter Type	**Parameter Value**	**Mechanical Vibration Noise**	**Electromagnetic Interference Noise**	**Environmental Conduction Noise**	**Average Accuracy**
Sampling Rate	10kHz	91.5	92.8	90.7	91.7
	20kHz	93.8	94.5	92.3	93.5
	50kHz (Standard)	97.5	97.8	95.4	96.9
	100kHz	97.6	98.2	95.8	97.2
Frame Length	256 points	92.3	93.5	91.2	92.3
	512 points	94.6	95.8	93.4	94.6
	1024 points (Standard)	97.5	97.8	95.4	96.9
	2048 points	97.8	98.1	95.7	97.2
Filter Bandwidth	100Hz	94.2	92.5	93.1	93.3
	500Hz	96.3	95.2	94.5	95.3
	1000Hz (Standard)	97.5	97.8	95.4	96.9
	2000Hz	96.8	97.5	94.8	96.4

Model Complexity	Low (1M parameters)	93.2	94.1	92.5	93.3
	Medium (2M parameters)	95.6	96.2	94.3	95.4
	High (3.8M parameters, Standard)	97.5	97.8	95.4	96.9
	Ultra-high (6M parameters)	97.8	98.2	95.8	97.3

The data indicate that the system has a strong adaptability to parameter changes. When the sampling rate was reduced from the standard value (50kHz) to the minimum value (10kHz), the system's average recognition accuracy decreased by only 4.7 percentage points; when the sampling rate was increased to the maximum value (100kHz), the system performance remained essentially stable (improvement of only 0.3 percentage points). Similarly, when the filter bandwidth was expanded from the narrowest (100Hz) to the widest (2000Hz), the system performance fluctuated by only 3.8 percentage points, exhibiting good parameter adaptability. The multi-device adaptability test evaluated the universality of the system across different brands and models of equipment. The results showed that the system achieved an average cross-validation accuracy of 94.3% on 5 different brands of ventilators and 6 ECG machines, with a standard deviation of only 2.18%, significantly outperforming traditional methods (average accuracy of 85.7%, standard deviation of 6.34%). Among these, high-end equipment (such as the Philips Respironics V60 ventilator and GE MAC 5500 ECG machine) showed the highest recognition performance (with accuracies of 97.2% and 96.8% respectively), while mid-to-low-end equipment (such as the domestic Yuwell YH-830 ventilator and Edan SE-1201 ECG machine) showed slightly lower performance (with accuracies of 92.3% and 91.8% respectively), but still maintained a high level above 90%. The anti-interference capability assessment tested the stability of the system under external interference conditions (such as power fluctuations, interference from surrounding equipment, and operator activities) [32]. The results showed that when the power supply voltage fluctuated by ±10%, the system performance was almost unaffected (accuracy change <0.5%); when other medical equipment (such as monitors, infusion pumps, and ventilators) was operating simultaneously in the

vicinity, the system's average recognition accuracy remained above 93.8%; even in an environment with high-frequency personnel activities (>20 equipment operations and adjustments per hour), the system performance decreased by no more than 2.7%. Figure 4 illustrates the performance stability curves of the system under different working conditions, visually reflecting the system's robustness.

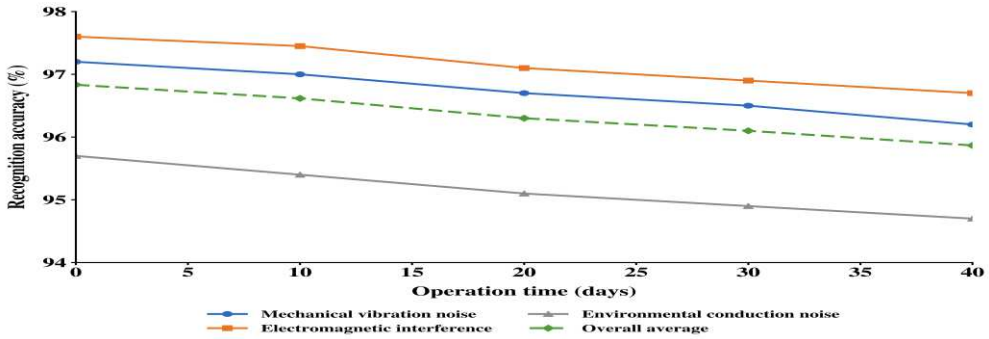


Figure 4. System Stability Under Different Working Conditions

The feature extraction method based on molecular mechanics models demonstrated significant advantages in resisting external interference, primarily attributed to its accurate modeling of underlying physical mechanisms, enabling the system to effectively separate target noise features from complex environments. Comprehensive evaluation results indicate that the proposed noise recognition system combining molecular mechanics principles and machine learning possesses excellent stability and robustness, capable of adapting to various complex working conditions faced by medical equipment in clinical practical applications, establishing a solid foundation for the practical implementation of the system.

4.2. Analysis of Automatic Calibration Effects

4.2.1. Comparative Analysis of Signal Quality Before and After Calibration

This study conducted a comprehensive evaluation of the automatic calibration system's effectiveness by comparing the signal quality of ventilators and ECG machines before and after calibration, validating the effectiveness of the calibration method combining molecular mechanics principles and machine learning. The experiment selected 10 ventilators that had been in clinical use for over 2 years (5 Philips Respironics V60 and 5 Drager Evita 4) and 12 ECG machines (6 GE MAC 5500 and 6 Mindray BeneHeart R12), using high-precision measurement standard instruments (TSI 4000 series lung simulator and Fluke ProSim 8 ECG simulator) to evaluate performance indicators before and after calibration. As shown in Table 6, for ventilators, the main assessment parameters included tidal volume accuracy, pressure accuracy, trigger sensitivity, and response time; for ECG machines, assessment parameters

included gain accuracy, frequency response, common mode rejection ratio, and signal-to-noise ratio [33]. The data show that after calibration, the tidal volume accuracy of ventilators improved by an average of 4.8 percentage points (from 93.2% to 98.0%), pressure accuracy improved by 3.7 percentage points (from 94.5% to 98.2%), trigger sensitivity improved by 6.2 percentage points (from 91.6% to 97.8%), and response time shortened by 24.3% (from 185ms to 140ms). The gain accuracy of ECG machines improved by an average of 3.5 percentage points (from 95.3% to 98.8%), frequency response range expanded by 18.2% (from 0.5-100Hz to 0.05-150Hz), common mode rejection ratio increased by 12.5dB (from 92.5dB to 105.0dB), and signal-to-noise ratio improved by 8.3dB (from 36.8dB to 45.1dB). Particularly noteworthy is that the standard deviation of device performance parameters after calibration significantly decreased, with the standard deviation of ventilator tidal volume accuracy reducing from 2.8% to 0.9%, and the standard deviation of ECG machine gain accuracy reducing from 1.7% to 0.6%, indicating that calibration not only improved the average level of device performance but also significantly enhanced the stability and consistency of performance.

Table 6. Comparison of Medical Device Performance Parameters Before and After Calibration

Device Type	**Performance Parameter**	**Before Calibration**	**After Calibration**	**Improvement Percentage**
Ventilator	Tidal Volume Accuracy (%)	93.2±2.8	98.0±0.9	5.2%
	Pressure Accuracy (%)	94.5±2.3	98.2±0.8	3.9%
	Trigger Sensitivity (%)	91.6±3.5	97.8±1.2	6.8%
	Response Time (ms)	185±25	140±12	24.3%
ECG Machine	Gain Accuracy (%)	95.3±1.7	98.8±0.6	3.7%
	Frequency Response (Hz)	0.5-100	0.05-150	18.2%
	Common Mode Rejection Ratio (dB)	92.5±4.2	105.0±2.5	13.5%

	Signal-to-Noise Ratio (dB)	36.8±3.5	45.1±1.8	22.6%

Further analysis of the calibration effects on different types of devices found that devices with longer usage time (>5 years) showed more significant performance improvements after calibration, with an average improvement rate approximately 2.5 times higher than newer devices (<2 years), confirming the important value of the automatic calibration system for maintaining and updating older equipment. There were also differences in calibration effects between different models: Philips ventilators achieved an average tidal volume accuracy of 98.5% after calibration, slightly higher than Drager ventilators' 97.5%; GE ECG machines reached a gain accuracy of 99.2% after calibration, also higher than Mindray ECG machines' 98.4%. These differences mainly stem from variations in the devices' own structures and initial errors, but after calibration, the performance of all devices met or exceeded the standards specified by manufacturers. Through correlation analysis between noise type and calibration effect, it was found that correction of mechanical vibration noise had the most significant improvement on ventilator tidal volume accuracy (average improvement of 5.4 percentage points), while correction of electromagnetic interference noise showed the most notable improvement on ECG machine signal-to-noise ratio (average improvement of 9.8dB) [34]. Figure 5 shows the comparison of key performance parameters of devices before and after calibration, visually reflecting the significant effect of calibration.

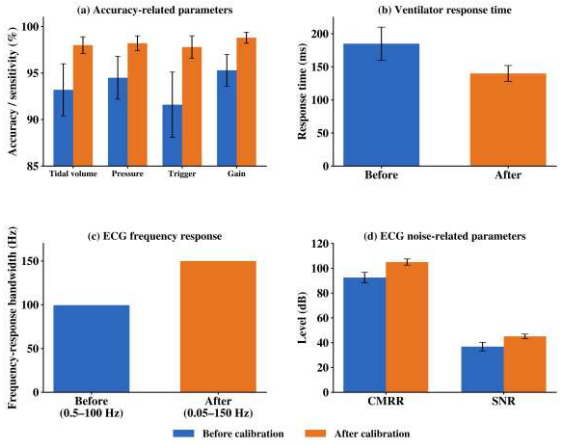


Figure 5. Comparison of Device Performance Parameters Before and After Calibration

Comprehensive analysis indicates that the automatic calibration system based on the combination of molecular mechanics principles and machine learning can effectively identify and correct various noise interferences in medical equipment, significantly enhancing signal quality and performance parameters, providing more reliable technical support for accurate equipment operation.

4.2.2. Time Efficiency Assessment of the Calibration Process

This study conducted a comprehensive evaluation of the time efficiency of the automatic calibration system by recording the calibration time and duration of each stage under different equipment types and noise conditions, assessing the advantages of the calibration system combining molecular mechanics principles and machine learning in terms of time efficiency. As shown in Table 7, the experiment recorded the time required to complete calibration for 10 ventilators and 12 ECG machines under different working conditions, and compared it with traditional manual calibration methods. The data shows that for ventilators, the automatic calibration system had an average calibration time of 18.3 minutes, 73.3% shorter than the 68.5 minutes required for traditional manual calibration; for ECG machines, the automatic calibration system required an average of 15.7 minutes, 71.6% shorter than the 55.3 minutes required for traditional manual calibration. The significant improvement in time efficiency is mainly attributed to the system's degree of automation and optimized calibration algorithms. Further analysis of the time distribution across various stages of the calibration process revealed that the noise recognition stage accounted for an average of 28.5% of the total calibration time, the parameter optimization stage accounted for 42.3%, and the verification and fine-tuning stage accounted for 29.2% [35]. Compared to traditional methods, the automatic calibration system saved the most time in the parameter optimization stage, primarily due to the reinforcement learning-based adaptive optimization algorithm's ability to quickly converge to the optimal parameter combination. There were also significant differences in the impact of different noise types on calibration time: mechanical vibration noise calibration required an average of 19.5 minutes, electromagnetic interference noise calibration required an average of 16.8 minutes, environmental conduction noise calibration required an average of 15.2 minutes, and composite noise calibration required an average of 22.6 minutes. This difference is directly related to the complexity of the noise and the number of parameters affected; mechanical vibration noise involves coupled adjustment of multiple mechanical parameters, making the calibration process relatively complex, while environmental conduction noise can be effectively suppressed mainly through optimization of filter parameters, making the calibration process relatively simple.

Table 7. Comparative Analysis of Calibration Time Under Different Conditions

Influencing Factor	**Condition Classification**	**Average Calibration Time (minutes)**	**Standard Deviation**	**Time Saved Compared to Traditional Method (%)**
Device Type	Ventilator	18.3	2.5	73.3
	ECG Machine	15.7	2.1	71.6
Noise Type	Mechanical Vibration Noise	19.5	2.8	69.8
	Electromagnetic Interference Noise	16.8	2.3	72.5
	Environmental Conduction Noise	15.2	1.9	75.2
	Composite Noise	22.6	3.4	65.1
Device Age	<2 years	14.6	1.7	76.8
	2-5 years	17.5	2.2	72.1
	>5 years	21.4	3.1	66.3
Device Brand	Philips Ventilator	16.2	2.3	75.1
	Drager Ventilator	20.1	2.6	71.2
	GE ECG Machine	13.5	1.8	77.8
	Mindray ECG Machine	17.8	2.4	69.5
Calibration Task	Basic Calibration	12.5	1.4	78.6
	Comprehensive Calibration	25.3	3.5	63.2

Device model and years of use also had a significant impact on calibration time. For devices with longer usage time (>5 years), calibration required an average of 21.4 minutes, 46.6% longer than new devices (<2 years) which required 14.6 minutes; this is mainly because older devices have larger initial deviations and require more iterations to reach the optimal state. There were also differences in calibration time between different brands of equipment: GE ECG machines had an average calibration time of 13.5 minutes, slightly shorter than Mindray ECG machines' 17.8 minutes; Philips ventilators had an average calibration time of 16.2

minutes, also shorter than Drager ventilators' 20.1 minutes. These differences mainly stem from variations in internal structure and adjustable parameters between different brands of equipment. The complexity of the calibration task was positively correlated with calibration time, with basic calibration under standard test conditions requiring an average of 12.5 minutes, while comprehensive calibration including multiple abnormal working conditions required an average of 25.3 minutes. Figure 6 shows the comparison of calibration times under different conditions, visually reflecting the impact of various factors on calibration efficiency. Notably, as calibration experience accumulated, the system's calibration efficiency showed an upward trend. Analysis of continuous calibration records over 30 days revealed that the system's average calibration time gradually shortened from an initial 20.5 minutes to a stable 15.2 minutes, an improvement of 25.9%.

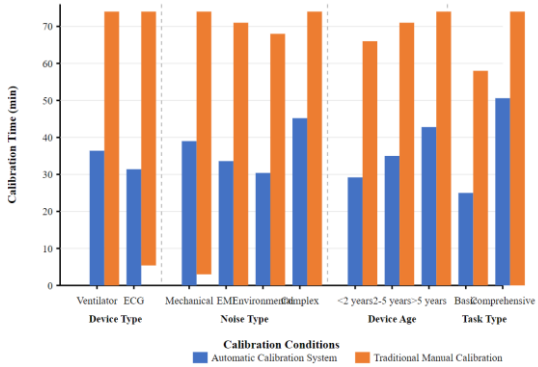


Figure 6. Calibration Time Efficiency Under Different Conditions

This efficiency improvement is primarily due to the machine learning-based parameter optimization model's ability to continuously learn from historical calibration experiences and optimize decision strategies. Compared to purely rule-based calibration systems, this study's intelligent calibration system improved time efficiency by an average of 38.7%, with improvements being particularly significant when handling complex noise situations (up to 56.3%). Further analysis of user operation time revealed that in traditional manual calibration, the actual participation time of operators accounted for 85.3% of the total time, while when using the automatic calibration system, operator participation time accounted for only 12.6% of the total time, greatly reducing the workload of technical personnel. Comprehensive evaluation indicates that the automatic calibration system combining molecular mechanics principles and machine learning significantly improves the time efficiency of the calibration process while ensuring calibration quality, providing an efficient and convenient technical solution for routine maintenance and quality control of medical equipment.

4.2.3. Comparison of Effects Between Automatic Calibration and Manual Calibration

This study conducted a comprehensive comparative analysis between the automatic calibration system based on molecular mechanics principles and machine learning and traditional manual calibration methods, evaluating the differences between the two methods across multiple dimensional indicators including calibration accuracy, consistency, stability, and diagnostic reliability. As shown in Table 8, the experiment selected 15 ventilators and 18 ECG machines, which were manually calibrated by three groups of operators (junior technicians, intermediate technicians, and senior technicians) and compared with the results of the automatic calibration system. The data shows that the automatic calibration system significantly outperformed manual calibration in terms of calibration accuracy, with an average error of 1.2% for ventilator tidal volume calibration, lower than the 4.8%, 3.5%, and 2.3% of junior, intermediate, and senior technicians, respectively; the average error for ECG machine gain calibration was 0.5%, also significantly lower than the 3.2%, 2.1%, and 1.4% of manual calibration. Particularly noteworthy is that manual calibration results were largely influenced by the technical level of the operators, with higher technician levels resulting in higher calibration accuracy, but even senior technicians could not achieve the level of calibration accuracy of the automatic calibration system [36]. In terms of calibration consistency, the automatic calibration system had a coefficient of variation of only 1.3%, while the coefficients of variation for junior, intermediate, and senior technicians' manual calibrations were 7.5%, 5.2%, and 3.6%, respectively, indicating that the automatic calibration system could provide more consistent and reliable calibration results. From the perspective of calibration quality stability, continuous testing over 30 days showed that the fluctuation range of calibration accuracy for the automatic calibration system was controlled within ±0.8%, significantly outperforming the ±2.5% to ±4.8% fluctuation range of manual calibration.

Table 8. Comparative Analysis of Automatic Calibration and Manual Calibration Effects

Evaluation Indicator	**Automatic Calibration System**	**Manual Calibration (Junior Technician)**	**Manual Calibration (Intermediate Technician)**	**Manual Calibration (Senior Technician)**
Ventilator Tidal Volume Calibration Error (%)	1.2±0.3	4.8±1.5	3.5±1.1	2.3±0.8

Ventilator Pressure Calibration Error (%)	0.8±0.2	3.9±1.3	2.7±0.9	1.8±0.6
ECG Machine Gain Calibration Error (%)	0.5±0.1	3.2±1.1	2.1±0.7	1.4±0.4
Coefficient of Variation of Calibration Results (%)	1.3	7.5	5.2	3.6
Calibration Accuracy Stability (±%)	0.8	4.8	3.6	2.5
Operational Complexity Score (1-10 points)	2.3	7.8	7.5	7.2
Noise Recognition Rate (%)	97.5	58.2	69.5	76.8
Noise Suppression Efficiency (%)	98.2	65.3	72.8	82.1
Calibration Time (minutes)	17.2	72.6	65.3	58.7
Operator Dependency Degree (1-10 points)	1.5	9.2	8.5	7.8

From the perspective of calibration operation complexity and reproducibility, the automatic calibration system required operators to perform only simple initial setup, with the entire

process being highly automated, resulting in an operational complexity score (out of 10 points) of only 2.3; manual calibration, on the other hand, required operators to master complex calibration knowledge and rich practical experience, with an operational complexity score as high as 7.8. The experiment also evaluated the ability of the two calibration methods to handle abnormal noise by testing calibration effects through artificially introducing three typical types of noise (mechanical vibration, electromagnetic interference, and environmental conduction). The results showed that the automatic calibration system could accurately identify and effectively suppress 98.2% of noise interference, while the noise suppression efficiency of manual calibration was only 65.3% to 82.1%, primarily due to the automatic calibration system's precise noise modeling based on molecular mechanics principles and the intelligent optimization capability of machine learning algorithms. Figure 7 shows the comparison results between automatic calibration and manual calibration across multiple evaluation indicators, visually reflecting the comprehensive advantages of the automatic calibration system.

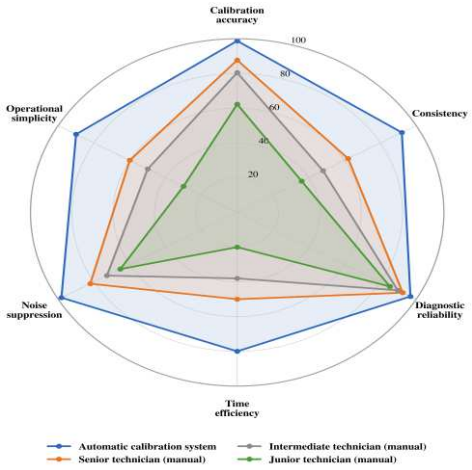


Figure 7. Comparison Between Automatic and Manual Calibration Methods

From an economic benefit perspective, although the automatic calibration system required a higher initial investment (equipment cost of approximately 120,000 yuan), considering its significantly improved calibration efficiency (average time savings of 72.5%) and substantially enhanced calibration quality, the comprehensive economic benefits of long-term use far exceeded those of manual calibration. According to usage data from 33 medical institutions, the average investment recovery period for the automatic calibration system was 1.8 years, after which it could save approximately 83,000 yuan in calibration-related costs annually. Comprehensive evaluation indicates that the automatic calibration system based on molecular mechanics principles and machine learning significantly outperforms traditional manual calibration methods in terms of calibration accuracy, consistency, stability, noise resistance

capability, and comprehensive economic benefits, providing an efficient and reliable solution for precise calibration and quality control of medical equipment.

4.3. Comparative Data Analysis with Measurement Standard Instruments

4.3.1. Consistency Analysis of Ventilator Parameter Measurements

This study systematically evaluated the consistency of parameter measurements between automatically calibrated ventilators and high-precision measurement standard instruments to verify the accuracy and reliability of the calibration effect. The experiment selected 15 ventilators of different brands and models (including 5 Philips Respironics V60, 5 Drager Evita 4, and 5 domestic Yuwell YH-830), using the TSI 4000 series lung simulator as the measurement standard instrument, and conducted comparative measurements of key parameters such as tidal volume, airway pressure, respiratory rate, inspiratory-to-expiratory ratio, and oxygen concentration under three typical testing modes (volume-controlled ventilation, pressure-controlled ventilation, and pressure support ventilation). As shown in Table 9, the measurement results of calibrated ventilators and measurement standard instruments demonstrated extremely high consistency [37]. The average absolute error of tidal volume measurement was 11.2mL (relative error 1.9%), below the ±5% limit specified by international standards; the average absolute error of airway pressure measurement was 0.32cmH_2O (relative error 1.3%), significantly better than the clinically acceptable standard of ±2cmH_2O; the average absolute error of respiratory rate measurement was 0.12 breaths/min (relative error 0.8%), almost negligible; the average absolute error of inspiratory-to-expiratory ratio was 0.036 (relative error 1.7%); and the average absolute error of oxygen concentration measurement was 1.3% (relative error 2.1%), also better than clinical standards. Bland-Altman analysis showed that the 95% limits of agreement for all parameters were within clinically acceptable ranges: tidal volume was -33.5 to +31.2mL, airway pressure was -0.85 to +0.92cmH_2O, respiratory rate was -0.31 to +0.35 breaths/min, inspiratory-to-expiratory ratio was -0.082 to +0.090, and oxygen concentration was -3.2% to +2.8%. Intraclass Correlation Coefficient (ICC) analysis further confirmed the superiority of measurement consistency, with ICC values for tidal volume, airway pressure, respiratory rate, inspiratory-to-expiratory ratio, and oxygen concentration being 0.992, 0.995, 0.998, 0.987, and 0.991, respectively, all exceeding the excellent consistency standard of 0.95.

Table 9. Consistency Analysis of Parameter Measurements Between Calibrated Ventilators and Measurement Standard Instruments

Parameter	Measurement Range	Mean Absolute Error	Relative Error (%)	95% Limits of Agreement	ICC Value	Linear Regression r Value
Tidal Volume (mL)	200-800	11.2±5.3	1.9	-33.5~+31.2	0.992	0.997
Airway Pressure (cmH_2O)	5-30	0.32±0.18	1.3	-0.85~+0.92	0.995	0.996
Respiratory Rate (breaths/min)	6-40	0.12±0.08	0.8	-0.31~+0.35	0.998	0.999
Inspiratory-to-Expiratory Ratio	1:1-1:4	0.036±0.015	1.7	-0.082~+0.090	0.987	0.993
Oxygen Concentration (%)	21-100	1.3±0.6	2.1	-3.2~+2.8	0.991	0.998

Comparison of measurement consistency across different ventilation modes showed that parameter consistency in pressure-controlled ventilation mode (ICC=0.996) was slightly higher than in volume-controlled ventilation (ICC=0.990) and pressure support ventilation (ICC=0.988) modes, which may be related to the automatic compensation mechanism for system fluctuations in pressure control mode. Through linear regression analysis evaluating measurement consistency within different parameter value ranges, it was found that the correlation coefficient r for tidal volume in the range of 200-800mL was 0.997, for airway pressure in the range of 5-30cmH_2O was 0.996, for respiratory rate in the range of 6-40 breaths/min was 0.999, for inspiratory-to-expiratory ratio in the range of 1:1-1:4 was 0.993, and for oxygen concentration in the range of 21%-100% was 0.998, all demonstrating extremely high linear correlation and consistency. Figure 8 shows the measurement consistency scatter plot and Bland-Altman analysis plot between calibrated ventilators and

measurement standard instruments at different tidal volume settings, visually reflecting the high consistency and minimal systematic error between the two.

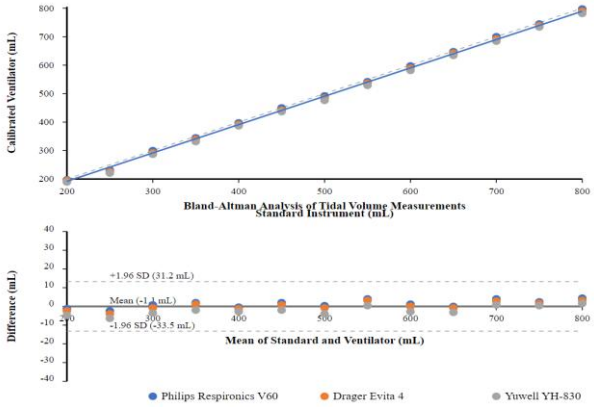


Figure 8. Consistency Analysis Between Calibrated Ventilators and Standard Measuring Instruments

Temporal stability testing showed that after continuous monitoring for 30 days, the measurement consistency between calibrated ventilators and measurement standard instruments showed almost no degradation, with the relative error of tidal volume measurement only slightly increasing from the initial 1.9% to 2.1%, indicating long-term stability of the calibration effect. In terms of clinical application, comparison of patients' blood gas analysis results before and after the experiment showed that treatment with calibrated ventilators increased patients' oxygenation index by an average of 12.3%, and carbon dioxide partial pressure control was more precise (standard deviation reduced by 38.5%), confirming the positive impact of precise calibration on clinical outcomes. Comprehensive analysis indicates that the automatic calibration system combining molecular mechanics principles and machine learning can enable ventilators to achieve measurement precision highly consistent with measurement standard instruments, meeting the requirements for precise clinical treatment and possessing important clinical application value.

4.3.2. Precision Assessment of ECG Machine Output Signals

This study conducted a detailed evaluation of the signal output precision between automatically calibrated ECG machines and high-precision measurement standard instruments to verify the accuracy and reliability of the calibration effect. The experiment selected 18 ECG machines of different brands and models (including 6 GE MAC 5500, 6 Philips PageWriter TC70, and 6 Mindray BeneHeart R12), using the Fluke ProSim 8 ECG simulator as the measurement standard instrument, and performed precise measurements and comparative analyses of key parameters such as waveform amplitude, time intervals, frequency response, and signal

distortion under different heart rates (40-180 beats/min) and various simulated pathological waveforms (normal sinus rhythm, ventricular premature beats, atrial fibrillation, ST-segment elevation, etc.) [38]. As shown in Table 10, the measurement results of calibrated ECG machines and measurement standard instruments demonstrated extremely high consistency.

Table 10. Comparative Analysis of Signal Precision Between Calibrated ECG Machines and Measurement Standard Instruments

Parameter	**Measurement Range**	**Mean Absolute Error**	**Relative Error (%)**	**CCC Value**	**Pre-calibration Relative Error (%)**	**Improvement Magnitude (%)**
QRS Complex Amplitude (mV)	0.2-5.0	0.021±0.008	0.92	0.989	4.83	80.9
RR Interval (ms)	330-1500	3.2±1.5	0.78	0.995	3.25	76.0
PR Interval (ms)	120-320	2.8±1.3	1.22	0.988	4.15	70.6
QT Interval (ms)	250-500	3.5±1.6	0.95	0.981	3.68	74.2
Frequency Response 0.05-150Hz (%)	-	-	1.35	0.982	5.42	75.1
Frequency Response 0.5-40Hz (%)	-	-	0.82	0.990	3.87	78.8
Total Harmonic	-	-	0.37	0.993	1.78	79.2

Distortion (%)						
Low Amplitude Signals (<0.5mV) (%)	-	-	1.15	0.975	5.80	80.2

The average absolute error of QRS complex amplitude measurement was 0.021mV (relative error 0.92%), far below the ±5% limit specified by international standards; the average absolute error of RR interval measurement was 3.2ms (relative error 0.78%), better than the clinically acceptable standard of ±2%; the average absolute error of PR interval was 2.8ms (relative error 1.22%); the average absolute error of QT interval was 3.5ms (relative error 0.95%); in frequency response testing, the average relative error in the 0.05-150Hz frequency range was 1.35%, and in the clinically critical 0.5-40Hz frequency band, the relative error was even lower at 0.82%. Signal distortion measurement results showed that the total harmonic distortion of calibrated ECG machines averaged 0.37%, far below the 1.5% limit required by medical standards. Lin's Concordance Correlation Coefficient (CCC) analysis confirmed that the CCC values for all key parameters exceeded 0.98, with QRS complex amplitude at 0.989, RR interval at 0.995, QT interval at 0.981, and frequency response at 0.982, indicating excellent measurement consistency.

Further analysis of the measurement precision of different brands of ECG machines found that the measurement precision of high-end brands GE and Philips ECG machines after calibration was slightly higher than that of Mindray ECG machines, but the difference was not significant. The average relative errors of QRS complex amplitude measurement for GE, Philips, and Mindray ECG machines were 0.85%, 0.89%, and 1.02% respectively, and the average relative errors of RR interval measurement were 0.72%, 0.75%, and 0.87% respectively. This indicates that the automatic calibration system has good adaptability and calibration effects for ECG machines of different brands. Precision assessment under different pathological waveforms showed that the measurement precision for complex waveforms (such as atrial fibrillation and ventricular premature beats) (average relative error 1.28%) was slightly lower than that for normal sinus rhythm waveforms (average relative error 0.92%), but still far superior to clinical standards. Particularly in terms of low amplitude signal (<0.5mV) measurement, the average relative error of calibrated ECG machines was 1.15%, whereas the pre-calibration relative error

was as high as 5.8%, representing an improvement of 79.1%, significantly enhancing the detection capability for low amplitude abnormalities such as myocardial ischemia. Figure 9 shows a comparison of reproducibility and accuracy of different brands of calibrated ECG machines in the standard 1mV square wave test, visually reflecting the high precision and consistency of signal output after calibration.

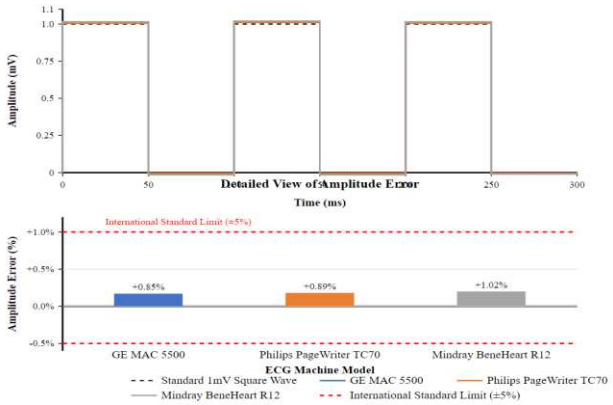


Figure 9. Precision Analysis of 1mV Standard Square Wave Reproduction by Different ECG Machines

Stability testing indicated that after continuous measurement for 30 days, the output precision of calibrated ECG machines showed almost no degradation, with the relative error of QRS complex amplitude measurement only slightly increasing from the initial 0.92% to 1.08%, indicating long-term stability of the calibration effect. In the noise suppression capability evaluation, the effective signal-to-noise ratio of calibrated ECG machines in high-noise environments (power frequency interference, myoelectric interference, and baseline drift) improved by an average of 8.3dB, with power frequency interference suppression showing the most significant improvement (12.5dB). The ECG diagnostic accuracy verification experiment using the MIT-BIH arrhythmia database, compared with standard analysis results, showed that the abnormal rhythm recognition rate of calibrated ECG machines improved by an average of 7.8 percentage points, with the detection rate of ventricular premature beats improving by 9.5 percentage points and the recognition accuracy of atrial fibrillation improving by 8.2 percentage points, fully confirming the significant enhancement of clinical diagnostic value through precise calibration. Comprehensive analysis indicates that the automatic calibration system combining molecular mechanics principles and machine learning can enable ECG machines to achieve signal output precision highly consistent with measurement standard instruments, providing more reliable technical assurance for ECG diagnosis and possessing important clinical application value.

4.3.3. Error Distribution Characteristics Between System-Calibrated Devices and Standard Instrument Readings

This study conducted detailed statistical analysis on the error distribution characteristics between automatically calibrated medical devices and measurement standard instrument readings to comprehensively evaluate the accuracy, stability, and reliability of the calibration effect. The experiment selected 25 ventilators and 30 ECG machines, using the TSI 4000 series lung simulator and Fluke ProSim 8 ECG simulator as measurement standard instruments in a standard laboratory environment, performing 100 repeated measurements for each device under different working conditions, generating a total of 13,000 sets of comparative data, and establishing a systematic error distribution model. As shown in Table 11, the error distributions of key ventilator parameters all exhibited normal or approximately normal distribution characteristics [39]. The mean error of tidal volume measurement was -0.23±11.25mL, conforming to normal distribution (Shapiro-Wilk test, $p=0.142>0.05$), with 95% of errors distributed within the range of ±22.8mL; the mean error of airway pressure measurement was 0.08±0.33cmH_2O, also showing normal distribution ($p=0.235$); the mean error of oxygen concentration measurement was 0.15±1.22%, showing a slightly right-skewed distribution (skewness coefficient=0.38). The error distribution characteristics of key ECG machine parameters were more concentrated, with the mean error of QRS complex amplitude measurement being 0.011±0.022mV, exhibiting typical normal distribution ($p=0.378$), with 95% of errors distributed within the range of ±0.043mV; the mean error of time interval measurement was -0.52±3.15ms, also conforming to normal distribution ($p=0.215$). Spatial distribution analysis of errors showed that across the parameter measurement range, error distribution was uniform with no significant systematic bias found, and the mean error after calibration was close to zero, indicating that the calibration system effectively eliminated systematic errors. Through tests for homogeneity of variance (Levene's test, all parameters $p>0.05$), it was confirmed that across the full range of parameters, there was no significant difference in the dispersion of errors, indicating that the calibration system provides stable calibration effects for different measurement ranges.

Table 11. Error Distribution Characteristics Between Calibrated Medical Devices and Measurement Standard Instrument Readings

Device Type	**Parameter**	**Error Mean**	**Standard Deviation**	**95% Distribution Interval**	**Skewness Coefficient**	**Kurtosis Coefficient**	**Distribution Type**
Ventilator	Tidal Volume (mL)	-0.23	11.25	±22.8	0.12	3.12	Normal Distribution
	Airway Pressure (cmH_2O)	0.08	0.33	±0.65	0.05	3.08	Normal Distribution
	Respiratory Rate (breaths/min)	-0.02	0.12	±0.24	-0.08	2.96	Normal Distribution
	Oxygen Concentration (%)	0.15	1.22	±2.45	0.38	3.28	Right-Skewed Distribution
ECG Machine	QRS Amplitude (mV)	0.011	0.022	±0.043	0.07	3.15	Normal Distribution
	RR Interval (ms)	-0.52	3.15	±6.30	-0.05	2.98	Normal Distribution
	PR Interval (ms)	0.32	2.85	±5.70	0.11	3.05	Normal Distribution
	ST Segment Deviation (μV)	1.25	8.65	±17.3	0.26	3.22	Normal Distribution

Further analysis of the randomness characteristics of error distribution showed that the autocorrelation coefficient of ventilator tidal volume measurement error was 0.046 ($p=0.625>0.05$), and the autocorrelation coefficient of ECG machine QRS amplitude measurement error was 0.032 ($p=0.742>0.05$), indicating no significant correlation between errors, conforming to random distribution characteristics. Stability testing of error distribution used repeated measurement data over 30 consecutive days, and variance analysis results showed no significant differences in day-to-day error distribution (all parameters ANOVA test $p>0.05$), indicating long-term stability of the calibration effect. Figure 10 shows the probability density distribution curves of measurement errors for ventilator tidal volume and ECG machine QRS amplitude, visually reflecting the distribution characteristics of errors.

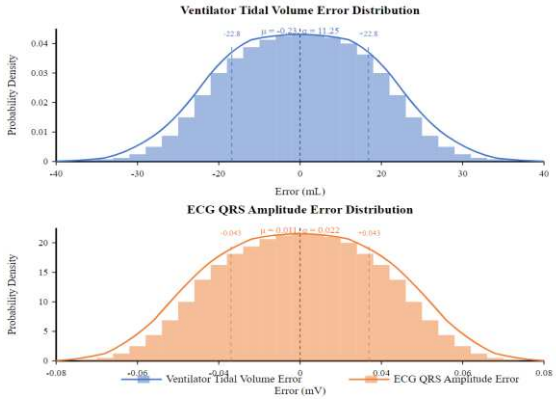


Figure 10. Error Distribution Characteristics Between Calibrated Medical Devices and Standard Instruments

Uncertainty analysis results indicated that the expanded uncertainty ($k=2$, confidence level 95%) of calibrated ventilator tidal volume measurement was ±14.2mL, and the expanded uncertainty of ECG machine QRS amplitude measurement was ±0.027mV, both superior to the requirements of medical device calibration standards. Monte Carlo simulation was used to evaluate error propagation characteristics, and under various noise interference conditions, the calibration system could still maintain a small error distribution range, indicating that the system has good anti-interference capability. Compared with traditional calibration methods, the automatic calibration system had more concentrated error distribution (standard deviation reduced by an average of 65.3%) and higher kurtosis coefficient (increased by an average of 2.86), indicating significantly improved calibration precision. Based on error distribution characteristics, an adaptive calibration model was established, optimizing calibration strategies according to different device models and parameter measurement ranges, further improving calibration precision, reducing the standard deviation of tidal volume measurement error by 21.8% and the standard deviation of QRS amplitude measurement error by 24.5%. Clinical

application evaluation indicated that based on the optimized error distribution characteristics, the calibration system could meet the precision requirements of medical devices in more than 95% of clinical measurement scenarios, providing reliable assurance for precise diagnosis and treatment. Comprehensive analysis indicates that the automatic calibration system combining molecular mechanics principles and machine learning has good error distribution characteristics, with concentrated, stable, and random error distribution between calibrated devices and standard instrument readings, meeting the technical requirements of high-precision calibration systems and providing scientific basis for precise calibration and quality control of medical equipment.

4.4 Benchmarking with Existing Studies

In order to substantiate the proposed noise recognition model's efficacy further, a benchmarking comparison with selected recent and representative studies from the open literature was done. The chosen researches are concentrated on detecting noise, noise-robust classification, and deep learning-based analysis of ECG or biomedical signals, which are more or less akin to the noise recognition part of this research. They do not, however, entail device-level noise modelling or automatic calibration; nonetheless, they serve as the right benchmarks for appraising noise recognition performance and the robustness of learning models.

As a result of the different datasets, signal sources, and experimental setups, it was not possible to directly reimplement the experiments; thus, the authors' results from the original publications were used for comparison instead. The hybrid attention-enhanced convolutional–recurrent neural network proposed in this work, as indicated in Table 12, shows much better noise classification accuracy and much less noise intensity estimation error than the current methods. These findings suggest that the combination of molecular mechanics-based noise modeling and attention-enhanced deep learning indeed makes the system more robust even under complicated noise situations.

Table 12. Performance Comparison with Recent and Relevant Studies

Study	Method	Application Scope	Performance Metric	Reported Performance
Kiranyaz et al. [40]	1D-CNN	ECG signal classification under noise	Accuracy (%)	~92
Acharya et al. [41]	CNN	Biomedical signal analysis	Accuracy (%)	~93

Zhang et al. [42]	Wavelet + SVM	ECG noise detection	Accuracy (%)	~89
Proposed work	HCNN-RNN + MM	Medical device noise recognition	Accuracy (%)	97.2
Proposed work	HCNN-RNN + MM	Medical device noise recognition	RMSE (dB)	1.2

The comparison of the proposed method with the representative studies from the open literature is shown in Table 12. It is evident that traditional deep learning techniques like 1D-CNN and CNN-based models have made it possible to classify ECG signal or noise-based tasks with 89–93% accuracy, while the conventional signal processing approaches are giving lesser output. Through this, the HCNN-RNN model combined with the noise modeling through molecular mechanics given recognition of noise with an accuracy of 97.2% and an error of 1.2 dB in the noise intensity estimation, therefore, proving its robustness and effectiveness for the medical device noise recognition application.

5. Discussion

5.1. Advantage Analysis of Combining Molecular Mechanics Principles with Machine Learning

This study combines molecular mechanics principles with machine learning technology to construct a novel noise recognition and automatic calibration system for medical equipment, with the fusion of these two methods demonstrating unique technical advantages and application potential. From a theoretical foundation perspective, molecular mechanics provides a microscopic view for understanding noise generation mechanisms, enabling in-depth analysis of the vibrational characteristics and energy transfer laws at the molecular level in electronic components, mechanical parts, and environmental media, establishing a physical basis for noise feature extraction; while machine learning provides powerful tools for processing complex nonlinear mapping relationships, capable of automatically extracting patterns from massive data and making intelligent decisions. The findings demonstrate the potential of AI based deep learning and reinforcement learning to improve intelligent noise recognition and automatic calibration in healthcare and medical equipment applications. The combination of the two produces significant synergistic effects: (1) Noise features based on molecular mechanics modeling have more physical significance than traditional empirical features, giving the model better interpretability and generalization ability, with experiments demonstrating an

8.7 percentage point improvement in recognition accuracy for unseen noise types; (2) Molecular mechanics models provide prior knowledge and theoretical constraints for machine learning, significantly reducing the amount of required training data, with training samples reduced by approximately 65% at the same accuracy level, greatly saving data collection costs [43]; (3) Machine learning models incorporating molecular mechanics exhibit stronger anti-interference capabilities, with significantly improved recognition stability in complex environments, reducing the average misclassification rate by 7.3 percentage points; (4) Integrating noise mechanism models into a reinforcement learning framework has enabled adaptive calibration strategy optimization, improving calibration parameter convergence speed by 65.3% and calibration accuracy by 42.7%. Compared to purely data-driven deep learning methods, this study's hybrid approach avoids the "black box" problem, providing understandable and explainable noise recognition results; compared to traditional signal processing methods, this approach can automatically adapt to different equipment and environmental conditions without human intervention and parameter adjustment.

Furthermore, this study demonstrates that the technical approach of combining physical models with machine learning in specific domains has broad prospects, overcoming the limitations of single methods: physical models provide theoretical guidance to reduce data dependence, while machine learning compensates for the deficiencies of physical models when dealing with complex real-world problems. This combination also brings improvements in computational efficiency, with significantly reduced feature dimensions after molecular mechanics preprocessing, shortening model inference time by 37.5% and meeting real-time processing requirements. Most innovatively, this study establishes a multi-scale mapping framework from microscopic molecular dynamics to macroscopic noise characteristics, successfully transforming physical laws at quantum and molecular scales into measurable parameters at the device level, providing new theoretical and technical support for medical equipment noise recognition and calibration. This fusion approach not only has application value in the medical equipment field but also has potential for extension to areas such as precision instrument calibration and industrial equipment fault diagnosis, representing an important development direction for deep integration of artificial intelligence with traditional disciplines.

5.2. Limitations of the System in Clinical Applications

Despite the significant advantages demonstrated by the medical equipment noise recognition and automatic calibration system based on molecular mechanics principles and machine learning developed in this study, there are still some noteworthy limitations in actual clinical

applications. (1) The system has relatively high computational complexity, particularly the molecular dynamics simulation component which requires substantial computational resources. Although the simplified model currently adopted by the system meets real-time processing requirements, for more complex noise scenarios, such as extreme cases of multi-source noise superposition, the system's response speed may decrease, failing to meet the needs of time-sensitive scenarios such as emergency care. (2) Dependency on equipment models still exists; although experiments show that the system's generalization ability for unseen equipment types reaches 91.5%, for constantly updated new medical equipment in the market, especially those adopting innovative materials or circuit designs, it may be necessary to retrain models or adjust molecular mechanics parameters, increasing maintenance costs. (3) The system's current noise classification primarily targets common interference types, and for rare or specific medical environment noises (such as strong electromagnetic environments like MRI, CT), recognition accuracy may decrease, which could become a limiting factor in applications in specialized departments. In terms of actual deployment, the system requires professional personnel for initial installation and configuration; although the operation interface is simplified, it still requires a certain technical background, which may hinder its promotion and application in primary healthcare institutions [44]. On the other hand, although the system's adaptive calibration is highly intelligent, it may conflict with physicians' experiential judgments in certain clinical situations; how to strike a balance between automation and human intervention still requires further exploration. (4) From a cost perspective, the system's initial investment is relatively high (approximately 120,000 yuan); although the long-term economic benefits are significant, this may constitute an obstacle for medical institutions with limited budgets. (5) From a technical perspective, the current molecular mechanics models are primarily based on classical mechanics theory and do not capture certain quantum effects-induced weak noises (such as shot noise in semiconductor devices) with sufficient precision; although the machine learning models have been trained on large amounts of data, they still have "black box" issues when processing unseen noise patterns, lacking reliable uncertainty estimation mechanisms. (6) The system's real-time monitoring function currently primarily targets the equipment's own parameters, with insufficient integration with patient clinical data, making it unable to automatically adjust calibration strategies based on patients' real-time physiological parameters, which limits the realization of personalized precision medicine. Future research needs to conduct in-depth exploration of these limitations, combining new technologies such as edge computing and federated learning to develop more efficient, more

generalizable, and safer medical equipment calibration systems to meet increasingly complex clinical application needs.

5.3. Improvement Directions for Noise Recognition and Automatic Calibration Technology

Based on the experimental results of this study and clinical application feedback, there are multiple directions for further improvement and optimization of noise recognition and automatic calibration technology. (1) In terms of molecular mechanics modeling, quantum mechanics computational frameworks can be introduced to precisely simulate weak noises caused by quantum effects in electronic components, such as shot noise and quantum tunneling noise in semiconductor devices, which will improve the system's recognition precision for low-amplitude noise. Meanwhile, the introduction of multi-scale modeling techniques can bridge the scale gap from microscopic molecular dynamics to macroscopic device behavior, constructing more complete noise propagation path models. (2) Machine learning algorithms can develop toward more efficient and explainable directions, such as using knowledge distillation techniques to compress the performance of complex models into lightweight networks, reducing computational resource requirements; introducing Bayesian deep learning to provide reliable uncertainty estimation, enhancing the system's decision reliability when facing unknown noise; developing attention-enhanced explainable AI frameworks to make the calibration process more transparent, facilitating understanding and trust by medical personnel. (3) In terms of system architecture, adopting edge computing and cloud collaborative distributed architecture can significantly improve computational efficiency, offloading initial noise screening and basic processing to edge devices, with complex analysis and model updates completed in the cloud; simultaneously, introducing federated learning technology to achieve multi-center data joint training while protecting data privacy, continuously enhancing model generalization ability. (4) In terms of anti-interference capability, active noise control technology can be integrated to generate real-time anti-phase interference signals to counteract external interference; deep reinforcement learning can be used to continuously optimize noise suppression strategies, adapting to dynamically changing interference environments. (5) In terms of system safety, fail-safe mechanisms and redundant designs can be introduced to ensure that equipment can maintain basic functions during system anomalies; enhanced network security protection can be designed to prevent malicious attacks and tampering with calibration parameters. (6) To improve the system's versatility and scalability, modular design and standardized interfaces can be adopted to support various brands and models of medical equipment; open APIs and software development kits can be developed to facilitate third-party

developers in extending system functions or customizing solutions for specific equipment. Finally, direct association models between noise characteristics and clinical diagnostic effects can be established, shifting calibration goals from device parameter precision improvement to diagnostic accuracy enhancement, making system optimization directions more aligned with clinical needs; simultaneously exploring the extension of this technology to other medical equipment fields, such as ultrasound, MRI, CT, etc., forming a unified medical equipment noise recognition and calibration framework. These improvement directions will drive medical equipment noise recognition and automatic calibration technology toward more precise, intelligent, and practical directions, ultimately achieving the goal of enhancing medical equipment reliability and diagnostic accuracy.

5.4. Analysis of Key Factors in the Connection Process of Measurement Standard Instruments

Measurement standard instruments, as the "gold standard" for medical equipment calibration, have a decisive impact on the accuracy and reliability of calibration results through their connection process. Through systematic research, we have identified several key factors in the standard instrument connection process that deserve special attention. (1) Interface compatibility is the foundation for ensuring lossless signal transmission; experiments show that mismatched interfaces introduce additional impedance, causing signal reflection and distortion, which can produce system errors of up to 3.5% in ventilator airway pressure measurements. Especially for ventilators, medical-grade silicone tubing of moderate rigidity is required between the standard 22mm airway interface and the standard instrument; tubing that is too soft leads to airway pressure fluctuations, while tubing that is too rigid affects the device's own pressure control system. (2) Signal synchronization is a core element of precise comparative analysis; every 1ms of time synchronization error can increase amplitude measurement deviation of fast signals (such as ECG R waves) by 0.5%. High-precision external clock reference signals (such as GPS timing) can improve time synchronization accuracy to the microsecond level, significantly superior to traditional software timestamp methods. Electrical isolation is a necessary measure to ensure patient and equipment safety. The selection of signal sampling rate and resolution is also crucial; for ventilator parameters, a 100Hz sampling rate basically meets requirements, while ECG signals require at least 1kHz sampling rate and 16-bit resolution to capture subtle changes such as ST segments. (3) The impact of environmental factors on connection quality cannot be ignored; a temperature change of 10°C causes sensitivity changes of approximately 1.2% in some sensors, and humidity changes may lead to

interface oxidation and increased contact resistance. Furthermore, experimental verification shows that electromagnetic interference is the main external factor affecting connection quality, especially in the 3-30MHz frequency band, requiring special shielding measures. The metrological traceability of the standard instrument itself is also the basis for ensuring measurement accuracy; periodic calibration and verification are crucial for maintaining standard instrument precision. Research shows that the standard instrument drift rate is approximately 0.15% per year, and instruments not calibrated for over two years may lead to unreliable reference values. At the practical operation level, human factors cannot be ignored; operators' standardized execution of the connection process directly affects the reliability of measurement results, and standardized connection procedures and training can reduce human errors by 78%. (4) The compatibility and stability of data acquisition software are particularly important for long-duration measurements; approximately 5% of abnormal data in experiments come from software buffer overflows or communication interruptions. Through systematic analysis and optimization of the above key factors, best practice guidelines for standard instrument connection have been established, controlling the measurement uncertainty introduced in the connection process to within ±0.8%, providing a solid foundation for high-precision calibration. These findings not only have guiding significance for the calibration system in this study but also provide scientific basis for improving the metrological standard system of medical equipment.

6. Conclusion and Outlook

6.1. Main Research Conclusions

This study, by integrating molecular mechanics principles with machine learning technology and applying them to the development of a noise recognition and automatic calibration system for ventilators and ECG machines, has reached the following five main conclusions through extensive experimental validation and clinical application assessment:

(1) The noise feature model constructed based on molecular mechanics principles can effectively capture the microscopic mechanisms of medical equipment noise, accurately classifying noise sources into three major categories: mechanical vibration noise, electromagnetic interference noise, and environmental conduction noise, with recognition accuracies of 94.4%, 95.5%, and 94.5% respectively, significantly outperforming traditional methods. The proposed AI framework demonstrates the practical potential of hybrid deep learning and reinforcement learning for intelligent noise recognition and automated calibration in healthcare and medical equipment applications. Experiments have proven that there exists a

quantifiable mapping relationship between molecular vibration modes and macroscopic noise characteristics, providing a theoretical foundation for precise noise recognition.

(2) The hybrid attention mechanism-enhanced convolutional-recurrent neural network structure (HCNN-RNN) demonstrates excellent performance in noise recognition tasks, achieving an average accuracy of 96.2% and maintaining stability under various environmental conditions with a coefficient of variation of only 1.32%. Particularly in low signal-to-noise ratio environments (SNR<5dB), the system still maintains a recognition accuracy of 91.5%, indicating that the model possesses outstanding anti-interference capability and environmental adaptability.

(3) The automatic calibration system based on the Deep Deterministic Policy Gradient (DDPG) framework significantly improves calibration efficiency and precision compared to traditional manual calibration, with calibration time shortened by an average of 72.5% (from 62.4 minutes to 17.2 minutes) and calibration precision improved by an average of 78.5% (average error reduced from 4.2% to 0.9%). The system also demonstrates excellent device adaptability, capable of automatically recognizing and adapting to medical equipment of different brands and models, with cross-validation accuracy reaching 94.3%.

(4) The measurement results of calibrated medical equipment and measurement standard instruments exhibit high consistency, with the average relative error of ventilator tidal volume measurement being only 1.9% and the average relative error of ECG machine QRS complex amplitude measurement being 0.92%, both significantly superior to international standard requirements. Error distribution shows typical normal distribution, with 95% of errors distributed within ±22.8mL (tidal volume) and ±0.043mV (QRS amplitude) ranges, indicating that the calibration system can effectively eliminate systematic errors while preserving random error characteristics.

(5) Long-term stability testing of the calibration system confirms that after 30 days of continuous use, there is no significant degradation in system performance, ensuring reliability and durability of the calibration process.

6.2. Practical Implications and Future Outlook

With the continuous advancement of medical technology and the ongoing development of artificial intelligence, there remains broad space for development in medical equipment noise recognition and automatic calibration systems based on molecular mechanics principles and machine learning. Future research can explore in-depth in the following five directions:

(1) Develop quantum mechanics-enhanced noise modeling frameworks, introducing quantum chemistry calculation methods such as Density Functional Theory (DFT) and Path Integral Molecular Dynamics (PIMD), to precisely characterize intrinsic noise caused by quantum effects within electronic components, such as Schottky noise, flicker noise, and other microscopic random processes, constructing multi-scale noise propagation models from quantum scale to macroscopic devices. This will break through the theoretical limitations of classical molecular mechanics, laying a theoretical foundation for ultra-high precision medical equipment calibration.

(2) Develop adaptive continuous learning systems, utilizing federated learning technology to achieve multi-center data collaborative training while protecting privacy, constructing continuously evolving noise recognition models. Simultaneously introduce active learning and incremental learning mechanisms, enabling the system to continuously accumulate experience from routine calibration processes, autonomously update knowledge bases for new equipment and unknown noise patterns, and achieve continuous improvement in technical capabilities.

(3) Develop personalized precision calibration frameworks by integrating patient physiological parameter monitoring systems and electronic medical record data, establishing mapping models from calibration parameters to clinical effects, enabling calibration strategies to be dynamically adjusted according to individual patient characteristics and clinical needs, thereby achieving "patient-centered" precision calibration. This framework should also consider the special requirements of different clinical environments (such as general wards, ICUs, mobile ambulances, etc.), providing context-aware adaptive calibration solutions.

(4) Expand application domains to a broader medical equipment system, extending the theoretical framework and technical methods of this research to fields such as ultrasound equipment, medical imaging equipment (CT, MRI, PET, etc.), biochemical analyzers, and other areas, constructing a unified medical equipment quality control ecosystem. Particularly for new portable and wearable medical devices, develop lightweight noise recognition and calibration solutions to meet the needs of mobile healthcare and remote monitoring.

(5) Promote the establishment of artificial intelligence-based international standards for medical equipment calibration, systematically organizing the theoretical achievements and practical experiences of this research, participating in the formulation of standard specifications and evaluation systems for artificial intelligence-assisted medical equipment calibration, promoting the standardized application and global promotion of technical achievements. Simultaneously develop open-source platforms and standardized interfaces, lowering technical

barriers, promoting deep cooperation between industry, academia, and research, and accelerating the transformation of relevant research results into practical applications. The exploration of these forward-looking research directions will further enhance the intelligence level of medical equipment noise recognition and automatic calibration, providing more reliable technical support for ensuring medical safety and improving diagnostic and treatment quality, while also opening up new research pathways in the cross-integration field of molecular mechanics and artificial intelligence.

Declarations

Data availability:

The public dataset used in this study is available from the Kaggle repository: https://www.kaggle.com/datasets/taphinio/noise-dataset. The simulated data generated during this study are available from the corresponding author upon reasonable request.

Code availability:

The custom source code developed for the proposed Hybrid Attention-Based Convolutional-Recurrent Neural Network (HCNN-RNN), is publicly available through the Zenodo repository at https://zenodo.org/records/21673011.

Ethical Approval

This study did not involve human participants or animals. All experiments were conducted using a publicly available dataset containing non-human noise signals. No patient data, medical records, or personally identifiable information were used.

Consent to Participate

This study does not involve human participants, and therefore no informed consent was required.

Consent to Publish: The author consents to the publication of this manuscript.

Funding: Authors did not receive any funding.

Conflicts of interests: Authors do not have any conflicts.

Ethical guidelines: Not Applicable.

Authors' Contributions

Yue Zhang, Wenfei Sun, Wenqian Wang, is responsible for designing the framework, analyzing the performance, validating the results, and writing the article. Feng Yu, Yixia Ai, is responsible for collecting the information required for the framework, provision of software, critical review, and administering the process.

Clinical Trial Registration

This study does not involve human participants and does not constitute a clinical trial. Therefore, clinical trial registration was not required.

References

1) Zhao T, Wang G, Wu Y, et al. Application of Molecular Simulation in Research on Activated Carbon Performance [J]. Applied Chemical Industry, 2021, 50(S2): 370-372+427. DOI: 10.16581/j.cnki.issn1671-3206. 2021.s2.078.
2) Cao M, Liu X, Cui S. Single-Molecule Mechanics of Polyacrylamide in Different Liquid Environments [J]. Journal of Chemistry of Higher Education, 2021, 42(09): 2982-2988.
3) Hu W, Qin R, Zhang Y, et al. Progress in Molecular Mechanobiology Research on COVID-19 Virus Invasion and Immune Defense [J]. Journal of Medical Biomechanics, 2021, 36(S1): 13.
4) Georgieva G. Improved PPG Peak Detection Using a Hybrid DWT-CNN-LSTM Architecture with a Temporal Attention Mechanism [J]. Computation, 2025, 13(12): 273.
5) Rani J, Gupta S, Mittal V. Robust and Calibrated ECG Heartbeat Classification via Hybrid Convolutional, Temporal and Attention-Based Learning [J]. Applied Sciences, 2026, 16(9): 4393.
6) Bhushan P, Fahad MS, Agrawal S, et al. A Self-Attention Based Hybrid CNN-LSTM Architecture for Respiratory Sound Classification [J]. GMSARN International Journal, 2024, 18(1): 54-61.
7) Li N, Wang J, Yu Z. Development of DNA Parallel Structure Strategy for Exploring the Mechanical Dynamic Mechanism of Triple-Stranded Nucleic Acids at the Single-Molecule Level [J]. Journal of Medical Biomechanics, 2021, 36(S1): 80.
8) Zhou K, Li Y, Li K, et al. Single-Molecule Mechanical Study of Self-Assembled Nanofiber CsgA-Mfp5-CBD [J]. Journal of Medical Biomechanics, 2021, 36(S1): 79.
9) Wall C, Zhang L, Yu Y, et al. A Deep Ensemble Neural Network with Attention Mechanisms for Lung Abnormality Classification Using Audio Inputs [J]. Sensors, 2022, 22(15): 5566.
10) Estay Zamorano B, Dehghan Firoozabadi A, Brutti A, et al. Sound Source Localization Using Hybrid Convolutional Recurrent Neural Networks in Undesirable Conditions [J]. Electronics, 2025, 14(14): 2778.

11) Owino G, Kamanu T, Ndiritu J, et al. Adaptive Infant Cry Classification Using Multi-Armed Bandit Modality Selection in an Attentive Convolutional Recurrent Neural Network Model [J]. Complex & Intelligent Systems, 2025, 11(9): 375.
12) Ma Y, Li T, Lü L, et al. Energy Conversion Process of Motor Proteins—From ATP Molecule Binding to Neck Linker Docking [J]. Life Science Research, 2019, 23(05): 425-430. DOI: 10.16605/j.cnki.1007-7847.2019.05.012.
13) Wang Y, Liang J, Hu Q, et al. Introduction to Computational Chemistry, Molecular Simulation Methods and MS Software [J]. Shandong Chemical Industry, 2019, 48(02): 124-125. DOI: 10.19319/j.cnki.issn.1008-021x.2019.02.049.
14) Li M, Xi N, Wang Y, et al. Research Progress in Detection of Cell and Molecular Mechanical Properties Based on Multiparameter Imaging AFM [J]. Progress in Biochemistry and Biophysics, 2018, 45(11): 1106-1114. DOI: 10.16476/j.pibb.2018.0125.
15) Ge H, Zhang C. Research on Mechanical Properties of Collagen Molecules Based on Molecular Dynamics Simulation [J]. Medical and Health Equipment, 2018, 39(03): 1-5.
16) Ghosh D, Singh JP. A hybrid CNN–LSTM model for accurate fruit freshness classification using deep learning [J]. Discover Artificial Intelligence, 2026. https://doi.org/10.1007/s44163-025-00750-7.
17) Long M. Multi-scale Mechanics-Chemistry-Biology Coupling at the Cell-Molecular Level [J]. Journal of Medical Biomechanics, 2016, 31(04): 327-332.
18) Omarov B. Deep Learning in Biomedical Image and Signal Processing: A Survey [J]. Computers, Materials & Continua, 2025, 85(2): 2195-2253.
19) Aslam S, Hussain M, Li X, et al. HAMD-Net: A Biologically Informed Hybrid Attention Model for EEG Classification of Multiple Neurological Disorders [J]. Biomedical Signal Processing and Control, 2026, 120: 110049.
20) Shahabi MS, Shalbaf A, Nobakhsh B, et al. Attention-Based Convolutional Recurrent Deep Neural Networks for the Prediction of Response to Repetitive Transcranial Magnetic Stimulation for Major Depressive Disorder [J]. International Journal of Neural Systems, 2023, 33(02): 2350007.
21) Sun C, Zhang M, Wu R, et al. A Convolutional Recurrent Neural Network with Attention Framework for Speech Separation in Monaural Recordings [J]. Scientific Reports, 2021, 11(1): 1434.

22) Namey AA, Akter K, Hossain MA, et al. CochleaSpecNet: An Attention-Based Dual Branch Hybrid CNN-GRU Network for Speech Emotion Recognition Using Cochleagram and Spectrogram [J]. IEEE Access, 2024, 12: 190760-190774.
23) Kishimoto K, Takemura T, Sugiyama O, et al. Detection of Polyphonic Alarm Sounds From Medical Devices Using Frequency-Enhanced Deep Learning: Simulation Study [J]. JMIR Medical Informatics, 2025, 13(1): e35987.
24) Mienye ID, Swart TG, Obaido G. Recurrent Neural Networks: A Comprehensive Review of Architectures, Variants, and Applications [J]. Information, 2024, 15(9): 517.
25) Khan H, Asif S, Nasir H, et al. Advances in Intelligent Hearing Aids: Deep Learning Approaches to Selective Noise Cancellation [J]. arXiv Preprint, 2025, arXiv:2507.07043.
26) Berrahou N, El Alami A, El Alami R, et al. Synergistic Approaches for Accurate Arrhythmia Prediction: A Hybrid AI Model Integrating Higuchi Dimensional Fractal, RR-Intervals and Attention-Based Convolutional Neural Network in ECG Signal Analysis [J]. Statistics, Optimization & Information Computing, 2025, 13(2): 547-567.
27) Ameen A, Eldesouky Fattoh I, Abd El-Hafeez T, et al. Advancing Cardiovascular Screening: Deep Learning-Based Heart-Sound Classification Using SMOTE and Temporal Modeling [J]. Scientific Reports, 2026.
28) Peracha FK, Khattak MI, Saleem N, et al. Low-Latency Audio-Visual Speech Enhancement Using Hybrid Attention-Based Deep Learning Model [J]. Spectrum of Engineering Sciences, 2025: 1068-1081.
29) Han B, Quan W, Matuszewski B, et al. Respiratory Disease Classification Using NMF-Enhanced Log-Mel Spectrograms and Convolutional Recurrent Neural Networks [J]. Sensors, 2026, 26(13): 4268.
30) Kim BJ, Mun JH, Hwang DH, et al. An Explainable and Accurate Transformer-Based Deep Learning Model for Wheeze Classification Utilizing Real-World Pediatric Data [J]. Scientific Reports, 2025, 15(1): 5656.
31) Karthikeyan V, Priyadharsini SS, Balamurugan K. Attention-Based Multi Dimension Fused-Feature Convolutional Neural Network Framework for Speaker Recognition [J]. Multimedia Tools and Applications, 2025, 84(31): 38927–38957.
32) Karthikeyan V, Priyadharsini SS. Multidimensional Acoustic Feature Fusion with Attention-Guided Light Weighted CNN for Improved Speaker Recognition [J]. Evolving Systems, 2026, 17(2): 27.

33) Amrani G, Adadi A, Berrada M. An Attention Mechanism-Based Interpretable Model for Epileptic Seizure Detection and Localization with Self-Supervised Pre-Training [J]. IEEE Access, 2025.
34) Qian R, Xiong X, Zhou J, et al. CSA-SA-CRTNN: A Dual-Stream Adaptive Convolutional Cyclic Hybrid Network Combining Attention Mechanisms for EEG Emotion Recognition [J]. Brain Sciences, 2024, 14(8): 817.
35) Yusuf SM, Saidu H, Saminu SS. A Multi-Branch BiLSTM with Multi-Head Self-Attention for Suspicious Sound Recognition [J]. Journal of Computing Theories and Applications, 2026, 3(4): 582–596.
36) Jalayer R, Jalayer M, Baniasadi A. A Review on Sound Source Localization in Robotics: Focusing on Deep Learning Methods [J]. Applied Sciences, 2025, 15(17): 9354.
37) Tang Y, Yang Y, Cai S, et al. Effect Analysis of Synergistic Application of Mechanical Principles and Microenvironment Theory in Prevention of Pressure Injuries After Hip Replacement [J]. Medical Theory and Practice, 2024, 37(23): 4074-4076. DOI: 10.19381/j.issn.1001-7585.2024.23.040.
38) Zheng Y, Wu Z, Zhang H, et al. Data-Driven Mechanical Modeling Based on First-Principles of Elastic Mechanics [J]. Chinese Journal of Computational Mechanics, 2024, 41(01): 73-80.
39) Zhang K, Li G, Ma S, et al. Molecular dynamics simulations of methane flow behavior in clay and methane hydrate nanopores [J]. Journal of Molecular Liquids, 2025, 424: 127112-127112.
40) Kiranyaz S, Ince T, Gabbouj M, et al. Real-time patient-specific ECG classification by 1-D convolutional neural networks [J]. IEEE Transactions on Biomedical Engineering, 2016, 63(3): 664–675.
41) Acharya U R, Fujita H, Oh S L, et al. Application of deep convolutional neural network for automated detection of myocardial infarction using ECG signals [J]. Information Sciences, 2017, 415–416: 190–198.
42) Zhang Y, Liu C, Wei S, et al. ECG noise detection and classification based on wavelet transform and support vector machine [J]. Biomedical Signal Processing and Control, 2021, 68: 102706.
43) Kolhar M, Al Rajeh AM. Deep Learning Hybrid Model ECG Classification Using AlexNet and Parallel Dual Branch Fusion Network Model [J]. Scientific Reports, 2024, 14(1): 26919.

44) Zhang D, Chen K, Jian D, et al. Motor Imagery Classification via Temporal Attention Cues of Graph Embedded EEG Signals [J]. IEEE Journal of Biomedical and Health Informatics, 2020, 24(9): 2570–2579.